Electronic Supplementary Information

Photo-activated CO-Releasing Molecules (PhotoCORMs) of Robust Sawhorse Scaffolds [μ^2-OOCR^1, η^1-$NH_2CHR^2(C{=}O]OCH_3$, $Ru(I)_2CO_4$]

Shuhong Yang, Mengjiao Chen, Lingling Zhou, Guofang Zhang, Ziwei Gao and Weiqiang Zhang*[a]

a. Key Laboratory of Applied Surface and Colloid Chemistry MOE, School of Chemistry and Chemical Engineering, Shaanxi Normal University, Xi'an 710062, China.

1. Crystal Data and Structure Refinement of Compound 3a, 3d, 3e and 3g

Intensity data collections were carried out with a Gemini E CCD diffractometer equipped with a CCD bidimensional detector using Mo-Kα (3a, 3e, 3g)and Cu-Kα (3d) monochromatized radiation (λ=0.71073 Å and λ=1.54178 Å respectively)[1]. The measurement was performed at 296 K. The absorption correction was based on multiple and symmetry-equivalent reflections in the data set using the SADABS program.[2] The structures were solved by direct methods and refined by full-matrix least-squares using the SHELX-TL package. CCDC:980017 (**3a**), 981493 (**3d**), 980018 (**3e**) and 980019 (**3g**) contain the supplementary crystallographic data for this paper. These data can be obtained free of charge from the Cambridge Crystallographic Data Centre via www.ccdc.cam.ac.uk/data_request/cif.

Table S1. Data Collection and Structural Refinements Details for Single-Crystal X-ray DiffractionStudies of Complexes 3a, 3d, 3e and 3g

compounds	**3a**·CH_2Cl_2	**3d**	**3e**	**3g**
empirical formula	$C_{15}H_{22}Cl_2N_2O_{12}Ru_2$	$C_{26}H_{28}N_2O_{14}Ru_2$	$C_{24}H_{24}N_2O_{12}Ru_2$	$C_{26}H_{28}N_2O_{12}Ru_2$
fw	695.39	794.64	734.59	762.64
T (K)	296(2)	296(2)	296(2)	296(2)
wavelength (Å)	0.71073	1.54178	0.71073	0.71073
Crystsyst	Triclinic	Triclinic	Monoclinic	Monoclinic
space group	P-1	P-1	P21/c	P21/c
a (Å)	8.0200(3)	9.9506(4)	11.2781(12)	11.6661(3)
b (Å)	12.3646(5)	12.5452(5)	15.2544(15)	15.7555(5)
c (Å)	13.3489(5)	13.6980(7)	19.7636(16)	19.8021(7)
α (°)	78.640(3)	96.569(4)	90	90
β (°)	82.951(3)	97.327(4)	124.796(4)	125.572(2)
γ (°)	76.046(3)	104.426(4)	90	90
V (Å^3)	1255.56(8)	1623.39(12)	2792.2(5)	2960.50(16)
Z	2	2	4	4
D_{calcd} (Mg·m^{-3})	1.839	1.626	1.747	1.711
absorp coeff (mm^{-1})	1.474	8.126	1.146	1.084
F(000)	688	796	1464	1528
Cryst size (mm^3)	0.14×0.13×0.09	0.14×0.12×0.11	0.16×0.14×0.09	0.13×0.12×0.09
*θ*range for data collection (deg)	3.12 to 26	3.29 to 67.49	3.37 to 25.10	3.32 to 26.00
index ranges	-9≤h≤9 -15≤k≤15 -16≤l≤16	-10≤h≤11 -15≤k≤14 -12≤l≤16	-12≤h≤13 -18≤k≤18 -23≤l≤22	-14≤h≤14 -15≤k≤19 -21≤l≤24
reflns collected	24960	12836	11631	13600
Indep reflns	4905 [R(int) = 0.0403]	5825 [R(int) = 0.0270]	4809 [R(int) = 0.0294	5810 [R(int) = 0.0315

completeness to θ	99.8 % (to 26)	99.8 %（to 67.49）	96.6% （to 25.10）	99.8 % (to 26.00)
max. and min. transmn	0.8788 and 0.8203	0.4685 and 0.3958	0.9039 and 0.8379	0.9087 and 0.8719
refinement method	Full-matrixleast-squareson F^2	Full-matrixleast-squareson F^2	Full-matrixleast-squareson F^2	Full-matrixleast-squareson F^2
data/restraints/params	4905 / 2 / 302	5825 / 0 / 401	4809 / 0 / 363	5810 / 43 / 367
GOF on F^2	1.102	1.051	1.064	1.072
final *R* indices	R1 = 0.0275	R1 = 0.0407	R1 = 0.0332	R1 = 0.0558
[$I > 2\delta(I)$]	wR2 = 0.0651	wR2 = 0.1019	wR2 = 0.0667	wR2 = 0.1384
R indices (all data)	R1 = 0.0373	R1 = 0.0515	R1 = 0.0471	R1 = 0.0792
	wR2 = 0.0716	wR2 = 0.1115	wR2 = 0.0741	wR2 = 0.1583
diff. peak and hole ($e \cdot Å^{-3}$)	0.563 and -0.639	1.500 and -0.522	0.535 and -0.383	1.849 and -1.233

Table S2. **Selected Bond Lengths (Å) for Complexes 3a, 3d, 3e and 3g**

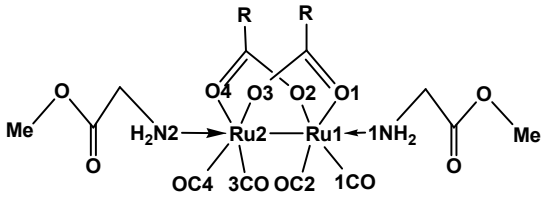

compounds	**3a**	**3d**	**3e**	**3g**
Ru(1)-C(1)	1.830(4)	1.843(5)	1.825(5)	1.822(7)
Ru(1)-C(2)	1.835(4)	1.846(6)	1.832(5)	1.833(8)
Ru(1)-O(2)	2.120(2)	2.130(3)	2.116(3)	2.113(4)
Ru(1)-O(1)	2.126(2)	2.133(3)	2.121(3)	2.114(5)
Ru(1)-N(1)	2.248(3)	2.271(4)	2.261(3)	2.270(6)
Ru(1)-Ru(2)	2.6760(3)	2.6803(5)	2.6742(5)	2.6754(7)
Ru(2)-C(3)	1.819(4)	1.835(5)	1.821(4)	1.833(8)
Ru(2)-C(4)	1.834(4)	1.840(5)	1.833(5)	1.843(9)
Ru(2)-O(3)	2.129(2)	2.119(3)	2.119(2)	2.123(4)
Ru(2)-O(4)	2.141(2)	2.122(3)	2.120(2)	2.128(6)
Ru(2)-N(2)	2.263(2)	2.249(4)	2.264(3)	2.261(6)
C(1)-Ru(1)-C(2)	89.69(16)	88.4(3)	89.75(19)	87.4(3)
C(4)-Ru(2)-O(3)	177.75(13)	179.21(18)	178.22(14)	178.7(3)
O(3)-Ru(2)-O(4)	84.28(9)	82.70(14)	85.29(10)	85.2(2)
N(1)-Ru(1)-Ru(2)	163.44(8)	161.22(10)	164.36(9)	162.86(19)
O(1)-Ru(1)-Ru(2)	85.16(6)	84.40(8)	84.65(7)	83.99(14)
O(2)-Ru(1)-N(1)	84.92(9)	84.14(12)	86.24(11)	83.5(2)
C(1)-Ru(1)-N(1)	95.91(12)	98.58(19)	95.00(16)	98.2(3)

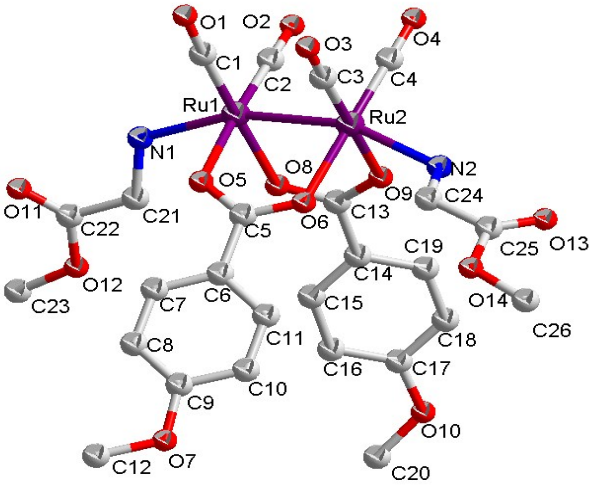

Fig. S1 Molecular structure of complex **3d.**

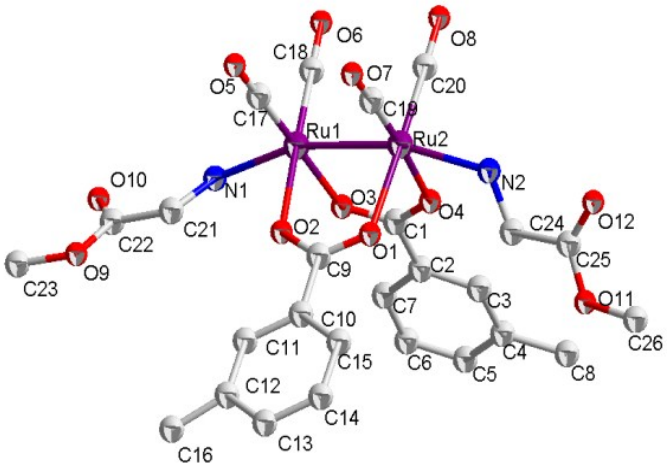

Fig. S2 Molecular structure of complex **3g.**

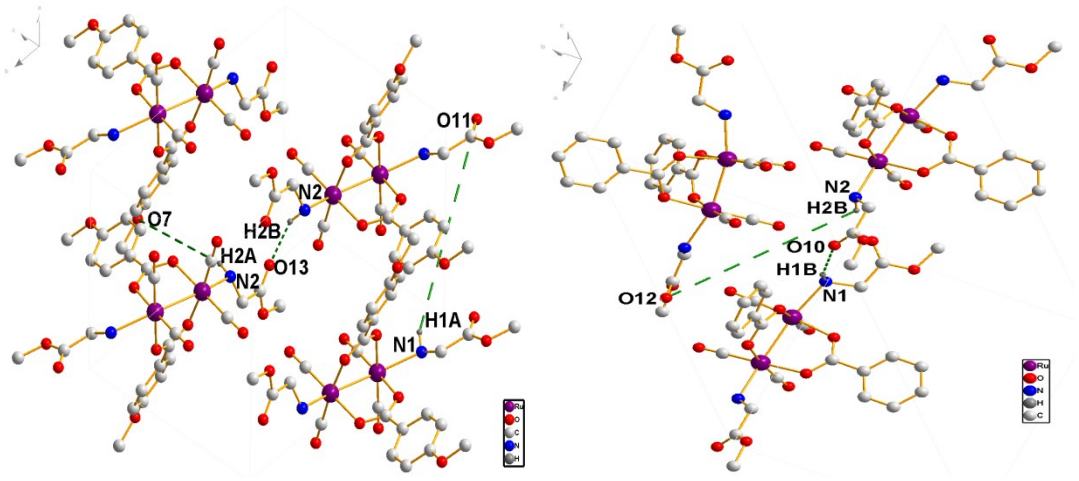

3d. 3e.

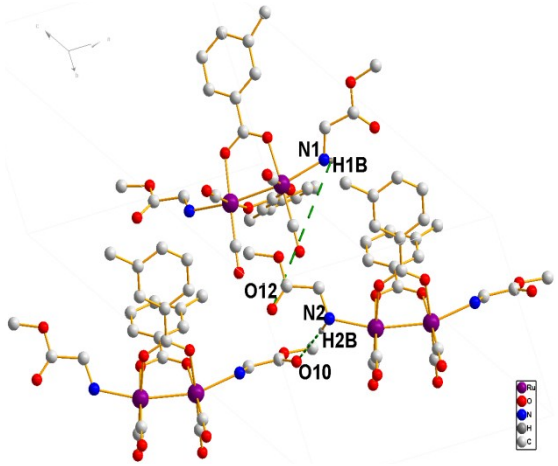

3g.

Fig. S3. Ball-and-stick diagram of the extended structure of **3d, 3e**and **3g**. Dashed lines indicate hydrogen bonding.

Table S3. Hydrogen bond distances (nm) and angles (°)

D-H···A	D(D-H)/nm	D(H···A)/nm	d(D···A)/nm	<(DHA)/ (°)
		3a		
N(1)-H(1B)…O(10) #1	0.90	2.23	3.093(4)	161
N(2)-H(2A)…O(4)#2	0.90	2.32	3.195(3)	163
N(2)-H(2B)…O(12)#3	0.90	2.30	3.137(4)	156
C(9)-H(9B)…O(8)#4	0.97	2.53	3.488(5)	168
C(12)-H(12B)…O(2)	0.97	2.37	2.995(4)	121
		3d		
N(1)-H(1A)…O(11) #1	0.90	2.45	3.078(6)	127
N(2)-H(2A)…O(7)#2	0.90	2.35	3.216(6)	161
N(2)-H(2B)…O(13)#3	0.90	2.17	3.002(6)	154
C(20)-H(20B)…O(4) #4	0.96	2.49	3.375(10)	153

C(21)-H(21A)…O(5)	0.97	2.56	3.161(6)	120
C(21)-H(21B)…O(8)	0.97	2.48	2.890(6)	105
C(24)-H(24A)…O(6)	0.97	2.36	2.937(7)	118
C(24)-H(24B)…O(3)#5	0.97	2.59	3.555(8)	174
		3e		
N(1)-H(1B)…O(10) #1	0.90	2.25	3.084(5)	153
N(2)-H(2B)…O(12)#2	0.90	2.08	2.954(6)	164
C(7)-H(7)…O(6) #3	0.93	2.55	3.269(8)	134
C(12)-H(12)…O(8) #4	0.93	2.54	3.442(6)	164
C(14)-H(14)…O(7) #5	0.93	2.56	3.277(8)	134
C(19)-H(19B)…O(1)	0.97	2.54	3.085(7)	116
C(21)-H(21B)…O(8)#5	0.96	2.56	3.298(6)	134
C(22)-H(22B)…O(2)	0.97	2.49	2.911(7)	106
		3g		
N(1)-H(1B)…O(12) #1	0.90	2.48	3.253(12)	145
N(2)-H(2B)…O(10) #2	0.90	2.15	3.041(14)	169
C(13)-H(13A)…O(5) #3	0.93	2.57	3.491(7)	169
C(21)-H(21B)…O(2)	0.97	2.53	2.961(18)	107
C(26)-H(26A)…O(5) #4	0.96	2.59	3.407(11)	143

Symmetry transformations used to generate equivalent atoms. For **3a**: #1 2-x,1-y,1-z; #2 1-x,2-y,-z; #3 -x,2-y,-z; #4 1+x,y,z. For **3d**: #1 -x,2-y,2-z; #2 1-x,2-y,1-z; #3 1-x,1-y,1-z; #4 1+x,1+y,z;#5 -x,1-y,1-z. For **3e**: #1 -1+x,y,z; #2 1+x,y,z; #3 1-x,1/2+y,3/2-z; #4 -x,-y,1-z;#5 x,1/2-y,-1/2+z. For **3g**: #1 1+x,y,z; #2 -1+x,y,z; #3 2-x,1-y,2-z; #4 x,3/2-y,1/2+z.

2. Photo-activated CO-Release Measured by Standard Myoglobin Assay

The release of CO from the metal carbonyl compounds was studied by measuring the conversion of deoxy-myoglobin (deoxy-Mb) to carboxy-myoglobin (Mb-CO). The amount of Mb-CO formed was quantified by measuring the absorbance at 540 nm. A stock solution of myoglobin (lyophilised horse heart) (66 μM final concentration) was prepared fresh by dissolving the protein in phosphate buffered saline (PBS) (0.01M, pH = 7.4). Sodium dithionite (0.1%) was added to convert the myoglobin stock to deoxy-Mb. A 2 mL quantity of this was measured to obtain a deoxy-Mb spectrum and then bubbled with CO to get a Mb-CO spectrum. CO-RMs were dissolved in an appropriate solvent (DMSO or EtOH) (4, 8, 12 μM) and added to deoxy-Mb in the cuvette (to give a final CO-RM concentration of 20, 40, 60 μM), mixed using a pipette and then overlaid with 500 μL light mineral oil to prevent CO escaping or the myoglobin being oxygenated.The cuvette was loaded in the chamber of UV spectrometer with an LED (365nm, 2.5W) on the top. The first spectrum (t=0s) was record without UV irradiation. The CO release were then initiated by UV irradiation. Each UV spectrum was record when LED turn off during scanning for a short time intervals. This is the standard procedure; other experiments have been undertaken using different concentrations of myoglobin and different concentrations of DMSO. The maximal absorption peak of deoxy-Mb at 560 nm is converted to the two maximal absorption peaks of Mb-CO at 540 and 578 nm. The concentration of myoglobin in the stock solution was calculated from the maximal absorption peak of the Mb-CO solution at 540 nm (Equation 1).

$$\textbf{Mb-COmax} = (\textbf{OD540} / \varepsilon) \times 1000$$

Equation 1. Equation for calculating total myoglobin concentration in a saturated solution of Mb-CO; ε = extinction coefficient of Mb-CO=15.4 $mM^{-1}cm^{-1}$, OD540 = absorbance of Mb-CO solution at 540 nm.

Intermediate concentrations of Mb-CO are calculated from the OD540. A new extinction coefficient (ε2) must be calculated to take into account the change in absorbance at 540 nm (ΔOD540). To aid in the accuracy of this calculation, another wavelength is used as a constant reference point. The deoxy-Mb and Mb-CO spectra share four isosbestic (ODiso) points (510, 550, 570, 585 nm). The value at 510 nm (ODiso510) was used in this set of experiments. The new extinction coefficient was calculated (Equation 2).

$$\varepsilon 2 = (\Delta\text{OD540} - \Delta\text{ODiso510} \times 1000) / \text{Mb-COmax}$$

Equation 2. Equation needed to calculate unknown Mb-CO extinction coefficient. ΔODiso510=change in absorbance at the isosbestic point, ΔOD540=change in absorbance at 540 nm, Mb-COmax=maximum concentration of myoglobin. ε2 = new extinction coefficient.

From the new extinction coefficient and the change in absorbance at 540 and 510 nm will give the concentration of myoglobin in any unknown sample. (Equation 3)

$$\text{Mb-CO} = 1000 \times (\Delta\text{OD540} - \Delta\text{ODiso510}) / \varepsilon 2$$

Equation 3. Equation to calculate the Mb-CO concentration in samples. ΔOD540 = change in absorbance at 540 nm, ΔODiso510 = change in absorbance at the isosbestic point, ε2 = calculated absorption coefficient. The resulting curves for the formation of Mb-CO verus time were fitted using non-linear regression routines in SigmaPlot, resulting R^2 values were typically greater than 0.99. Half lives for CO-release were determined by extrapolating the equations generation from the non-linear regression to 30μM, 20μM and 10μM Mb-CO for initial CORM concentrations of 60 μM, 40 μM and 20 μM respectively. The same method was employed for CORM which exhibited slow release for Mb-CO concentrations of 15μM, 10μM and 5μM respectively. In the case of complexes 3a-3g significant baseline drift was observed in the Mb-CO assay which was corrected with the aid of a non-linear regression algorithm being applied to the isosbestic points [3].

3. Mechanistic Experiments on Photo-activated degradation of 3a

3.1 Thermogravimetric Analysesof 3a and XPS of Inorganic Residue

Thermal stability studies of **3a** were collected on a METTLER TOLEDO TGA/SDTA851^e TGA analyzer with a heating rate of 10℃/min from 25℃ to 800℃ under nitrogen atmosphere.

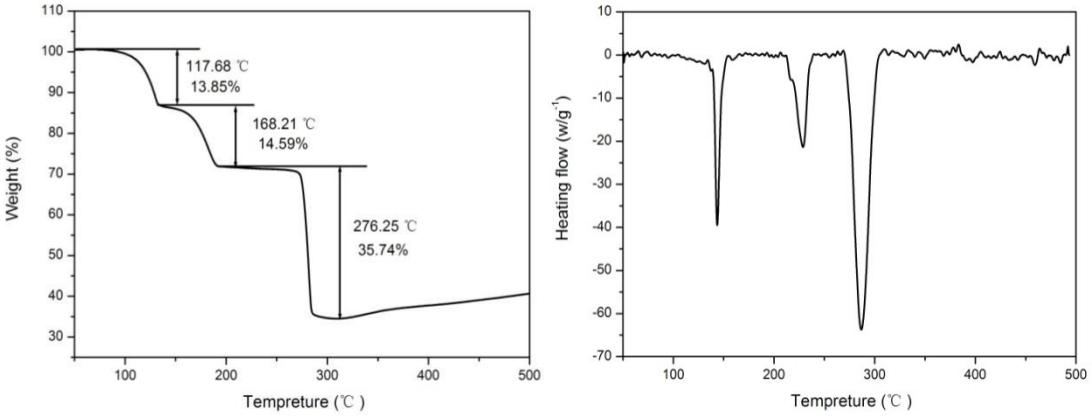

Fig. S4 TGA/DSC analysis of **3a**.

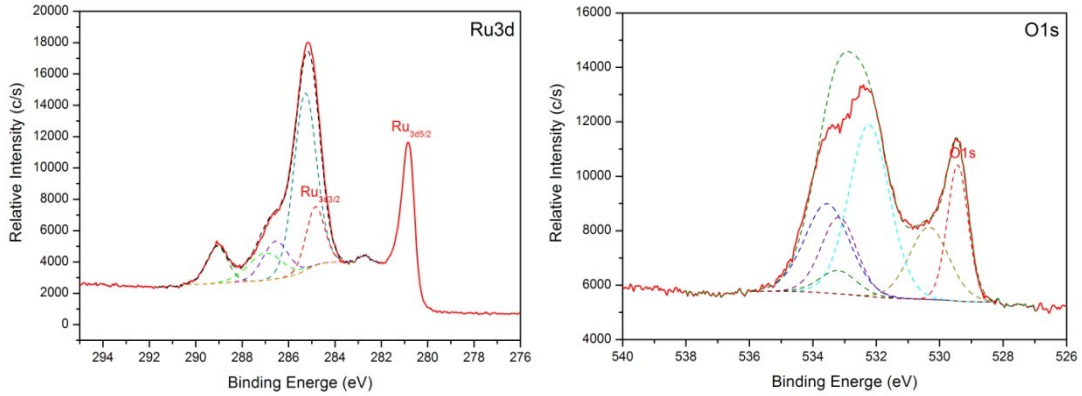

Fig. S5 XPS patterns of inorganic residue (red solid line); The dotted line represents the fitting results.

Table S4. Binding Energies and Valences of the inorganic residue

electron level	binding energy (eV)	valence
Ru3d5/2	280.8	+4
Ru3d3/2	284.8	
O 1s	529.4	-2

Figure S5 is the XPS pattern of the product. The resultsof Ru3d5/2, Ru3d3/2, and O 1s electron binding energiesare shown in Figure S5 and Table S4, which are identical to the values recorded in the database. Through the calculation of peak area, the atomratio of Ru and O is about 1:2. As seen in Table S4, the valences of Ru and O are +4 and -2 in proper order.

3.2 FT-IR Experiments of Photoactivated degradation of 3a

CORM 3a (1mg) wasdissolved with the delivery solvents (1mL) at 25 °C. The CORM solution was then loaded in the liquid cell equipped with CaF_2 window and PTFE spacers (0.1mm). Each IR spectrum was record after the irradiation with an LED (at 365nm 2.5W) for a certain time interval.

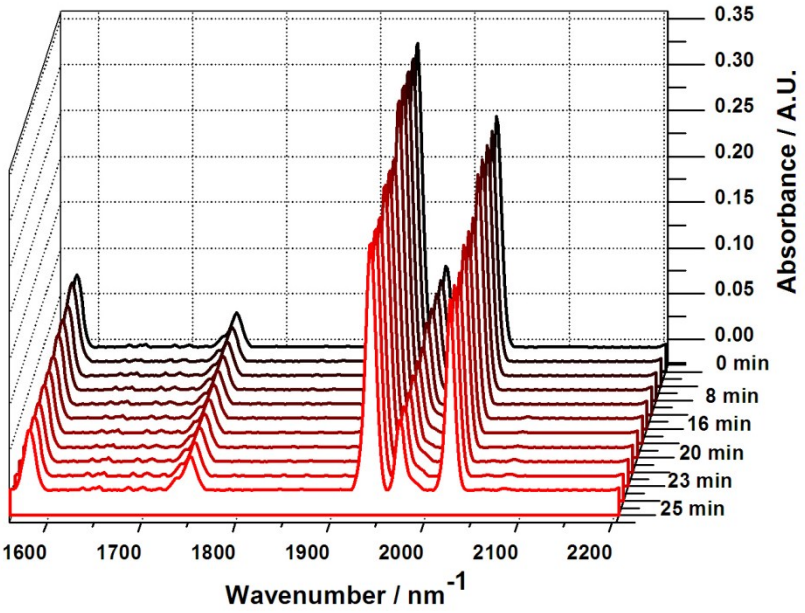

Fig. S6 FT-IR spectrum ($\nu_{(CO)}$region) of complex **3a** in methanol solution and the changes that occur during 365 nmphotolysis.

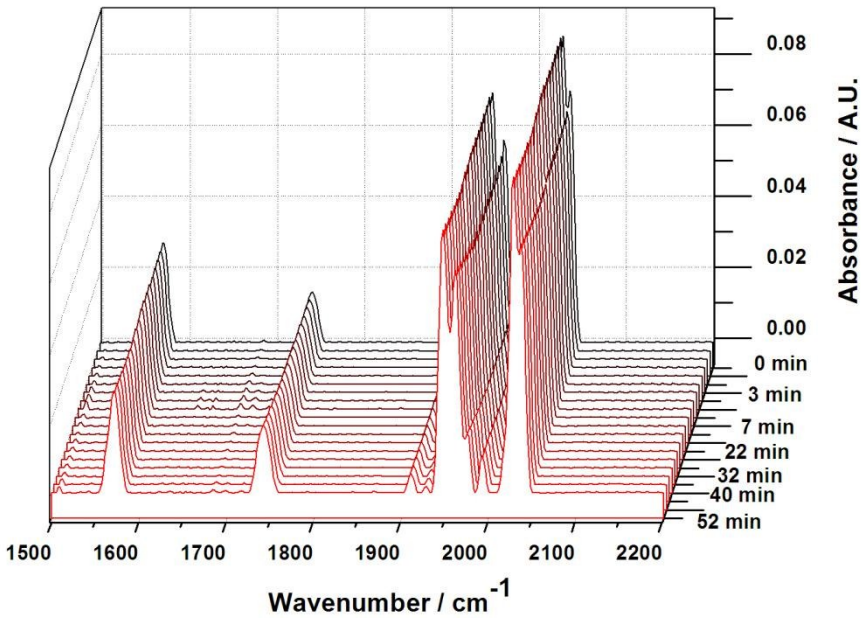

Fig. S7 FT-IR spectrum ($\nu_{(CO)}$region) of complex**3a** in DMSO solution and the changes that occur during 365 nmphotolysis.

3.3 NMR Experiments of photoactivated degradation of 3a

CORM3a (10 mg) was dissolved in CD_3CN (0.5 mL). A ^{1}H-NMR spectrum was acquired immediately after addition, and then the sample monitored for a total of 101 minutes under UV irradiation. The resulting spectra are shown in Fig. S8.

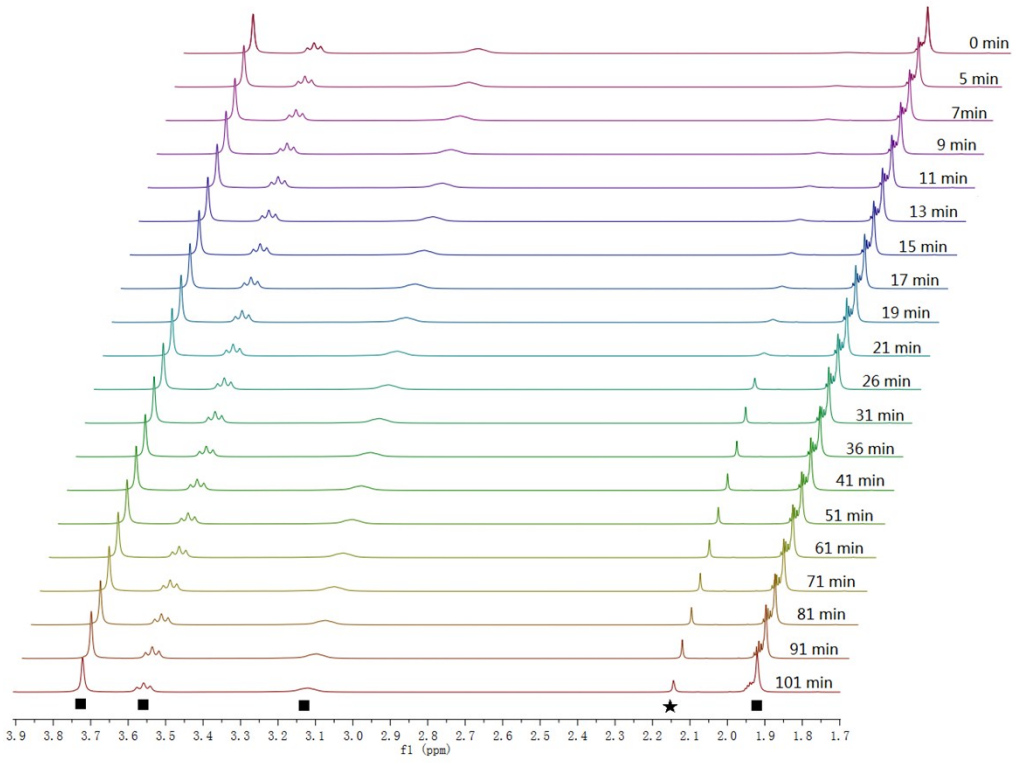

Fig. S8 Evolution of the ^{1}H NMR spectra (1.7 – 3.9 ppm region) of a solution of **3a** (■)in CD_3CN under irradiation at λ_{irr}= 365 nm, photo product (★).

3.4 GC-MSAnalysis on 3a after Photolysis

After photolysis by an LED for 370 min, the acetonitrile solution of 3a was diluted with methanol solution (60ug/mL). The sample was analysis by Bruker SCIONTQ GC-MS/MS.

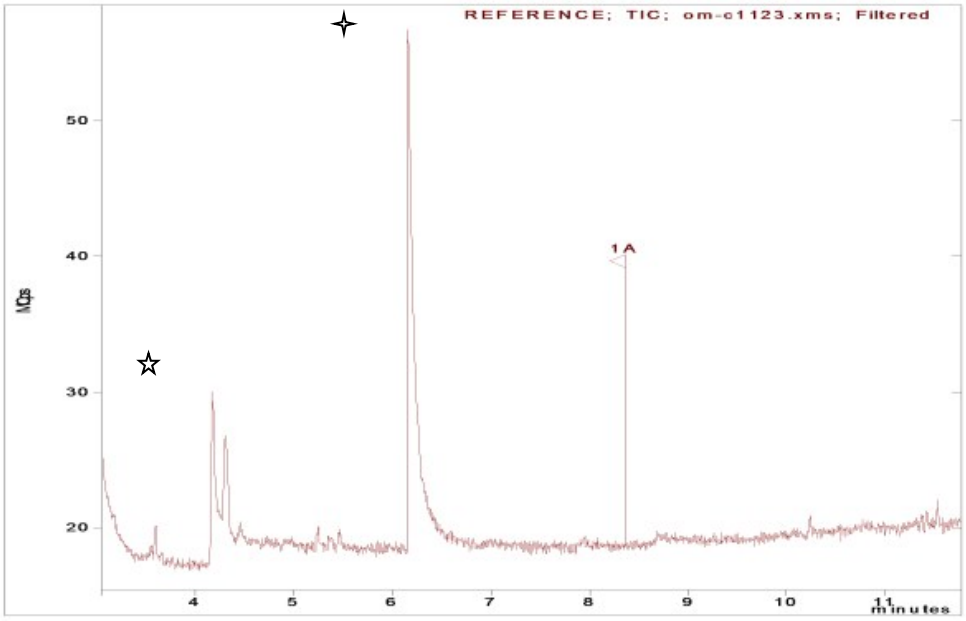

a. GC spectrum of organic degraded products after photolysis of 3a

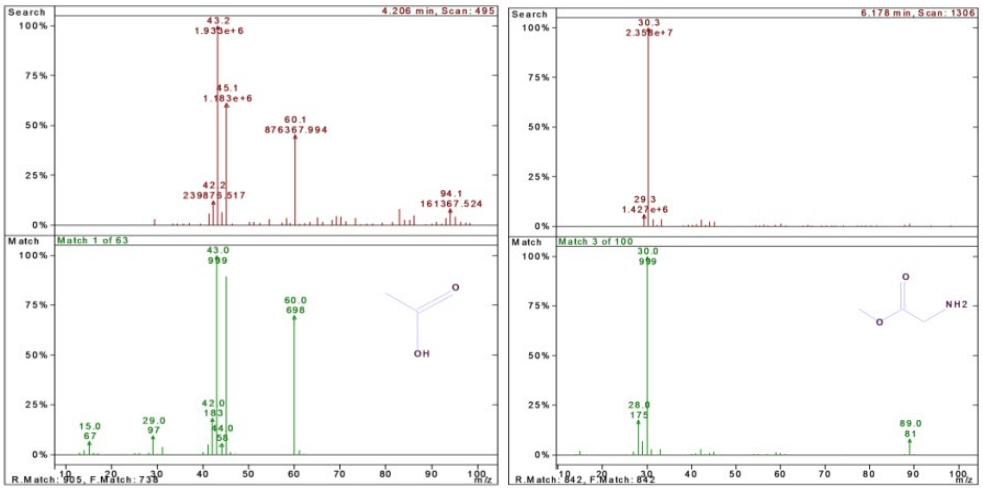

b. MS identification on peak (☆) at Rt 4.2min and peak (✧) at Rt 6.1 min

Fig. S9 GC-MS spectrum of photolysis products of compound 3a, acetic acid (☆) and GlyOMe (✧) were identified by MS

3.5 Mass Spectrometer studies on photolysis of 3a

An UV LED (365nm, 2.5w) was set above the syringe containing acetonitrile solution of **3a**. The subsequent photolysis reaction were monitored online by ESI-MS. **Fig. S10-(1)** is the mass spectra of complex 3a without UV irradiation. The resulting spectra are shown respectively in **Fig.S10-(2)-(9)**.

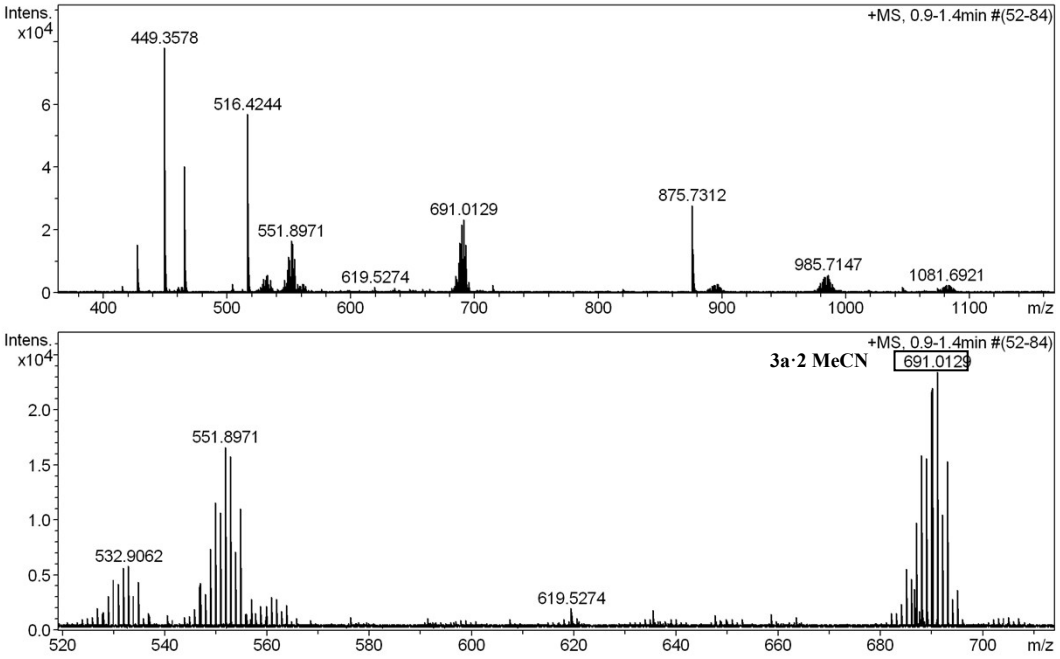

Fig. S10-(1)

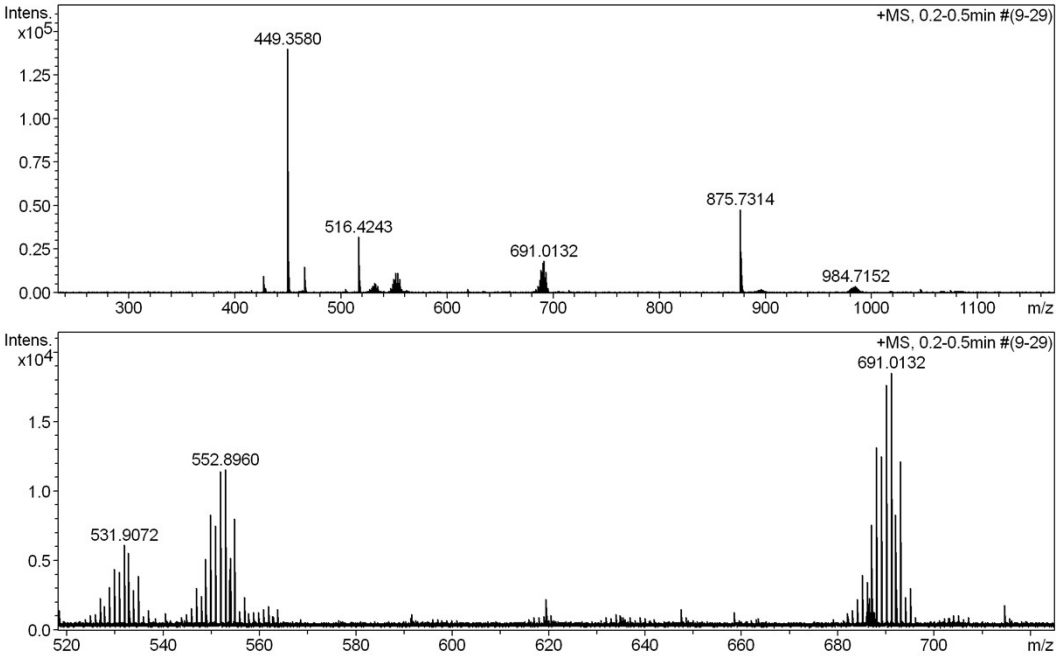

Fig. S10-(2)UV irradiation for5 minutes

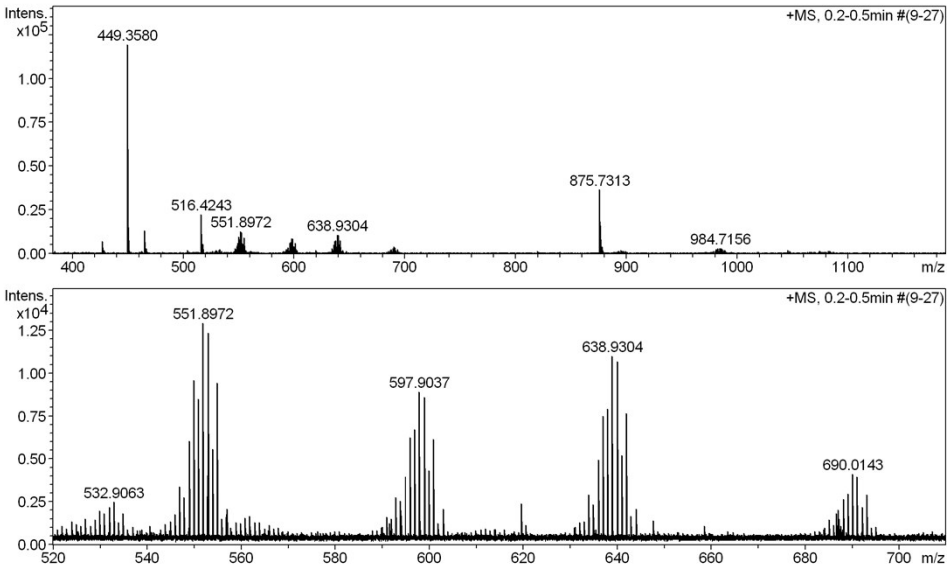

Fig. S10-(3)UV irradiation for8 minutes

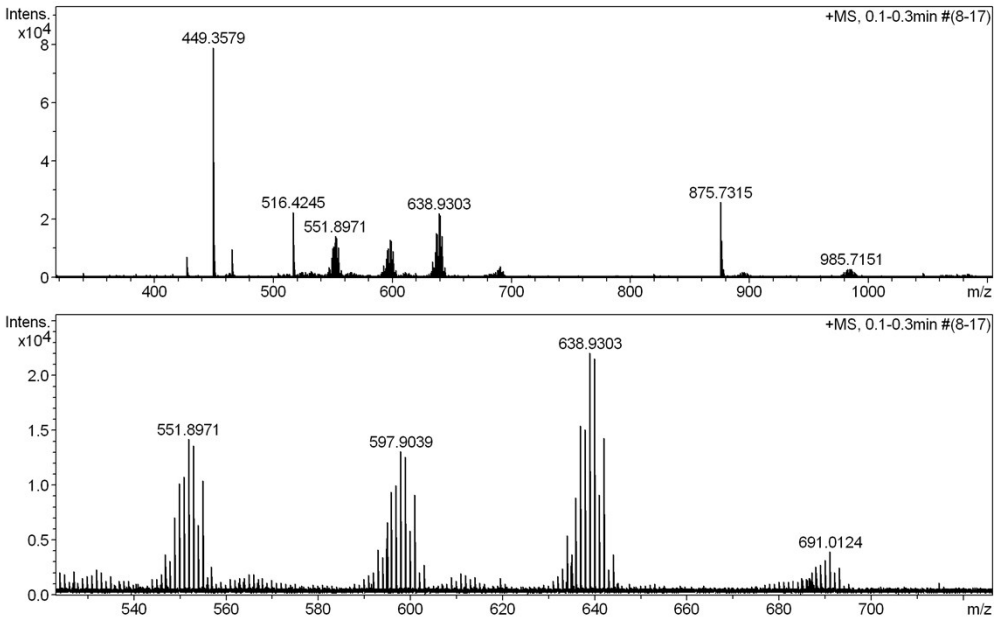

Fig. S10-(4)UV irradiation for10 minutes

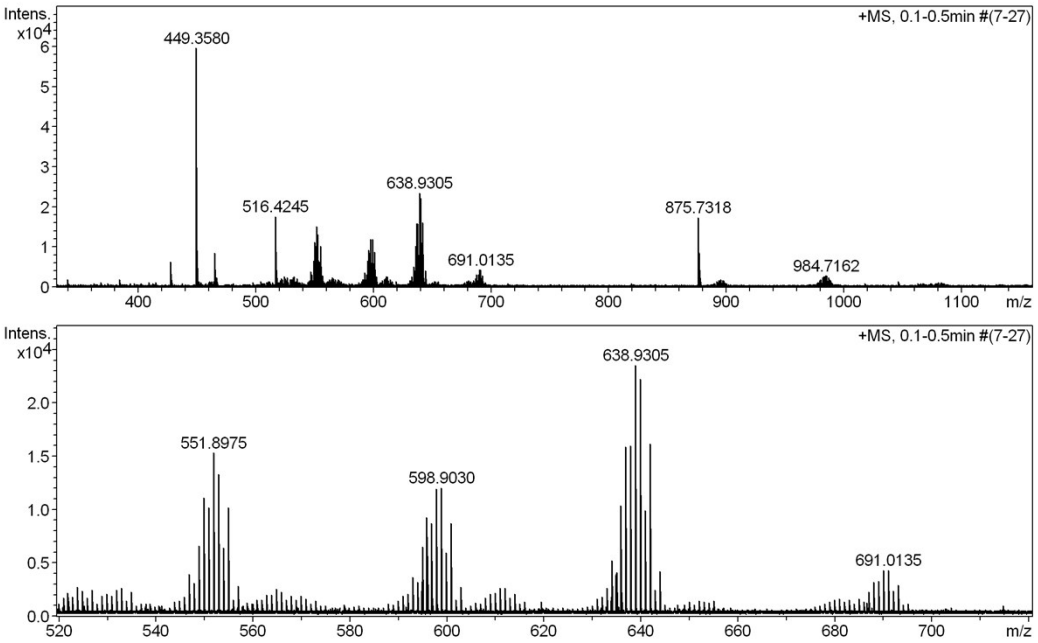

Fig. S10-(5)UV irradiation for11 minutes

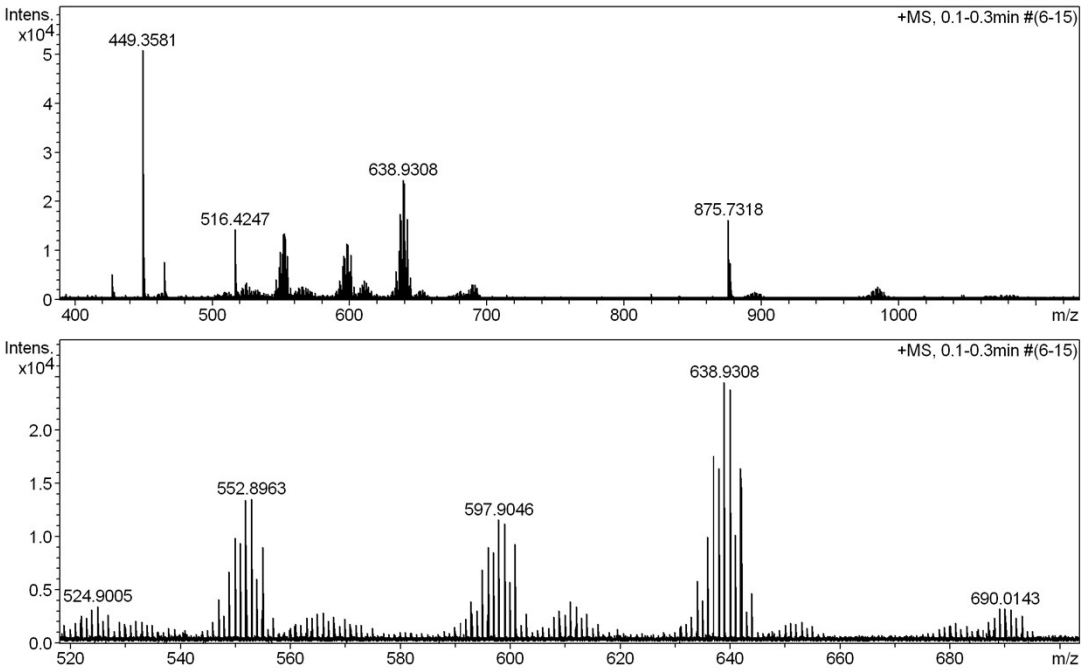

Fig. S10-(6)UV irradiation for 12 minutes

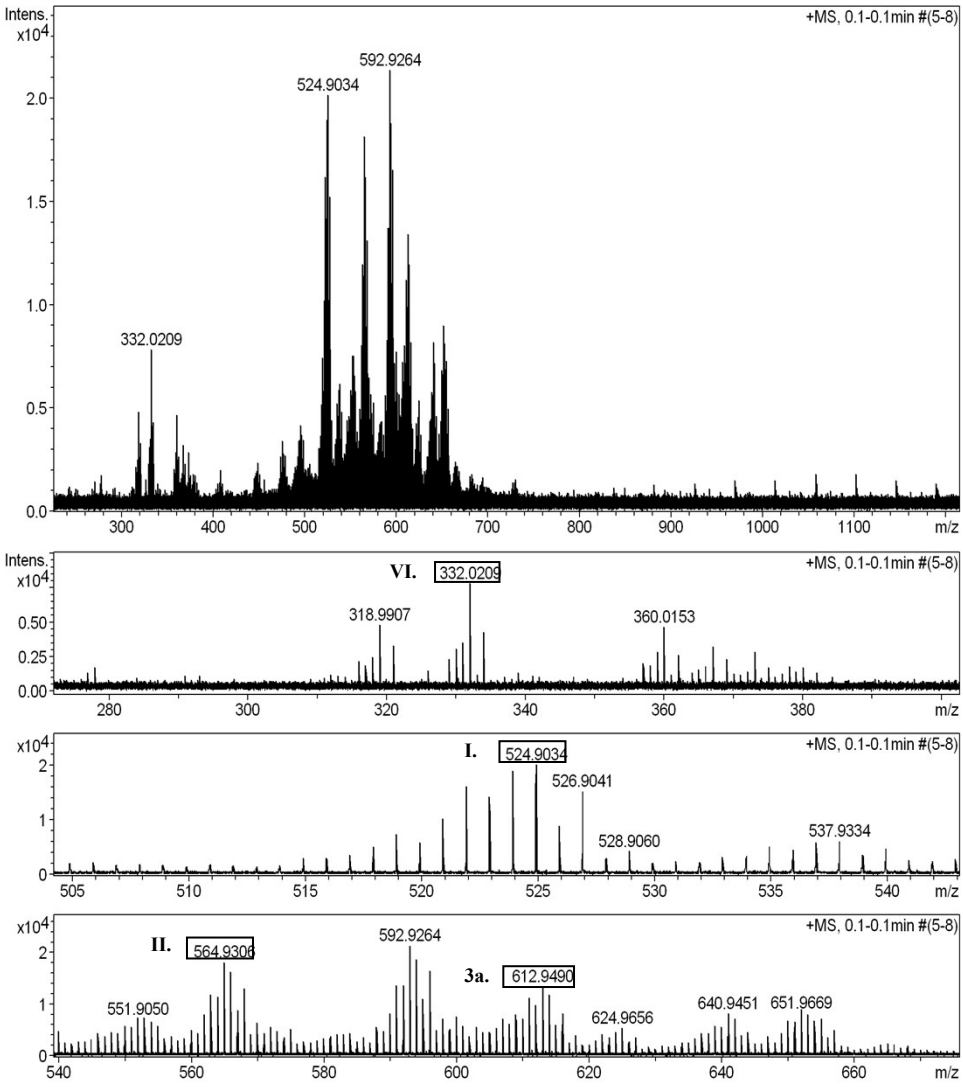

Fig. S10-(7)UV irradiation for 15 minutes

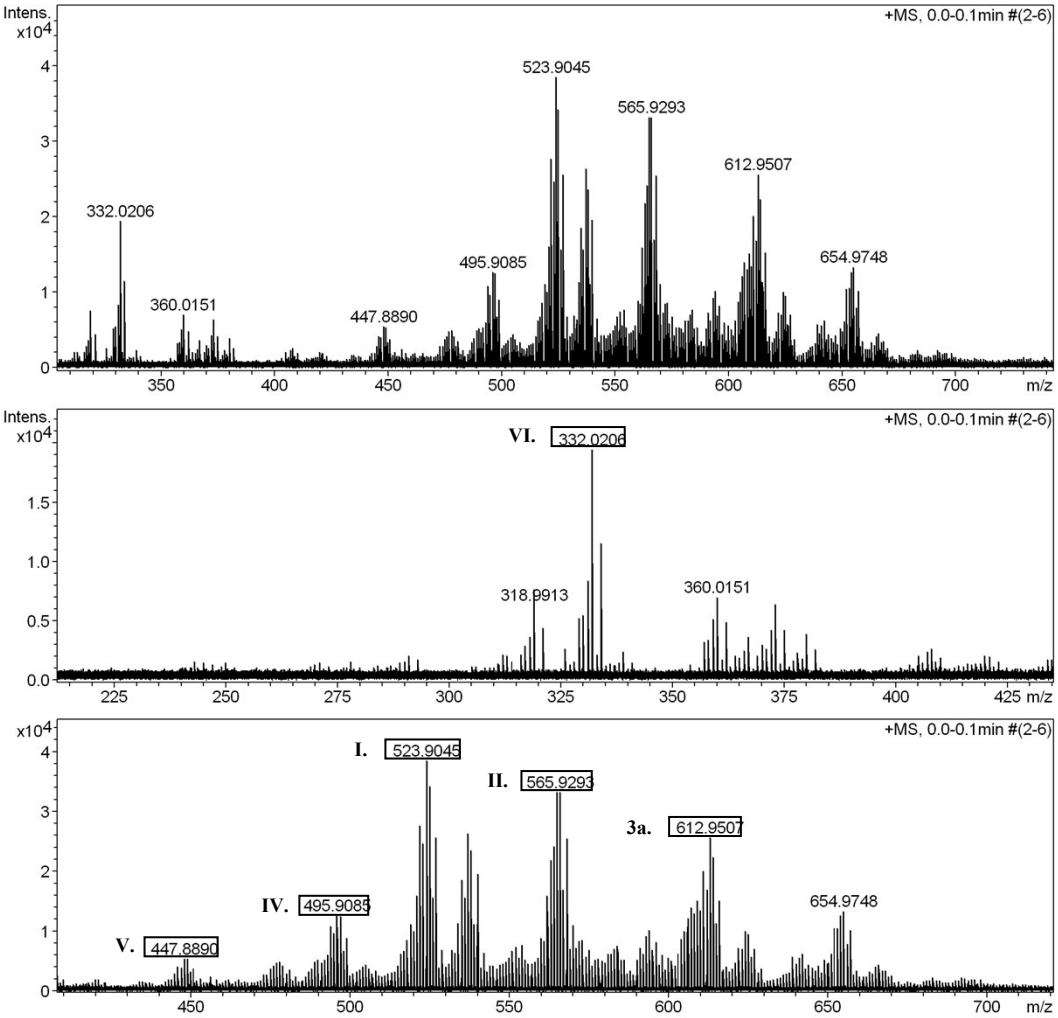

Fig. S10-(8)UV irradiation for 30 minutes

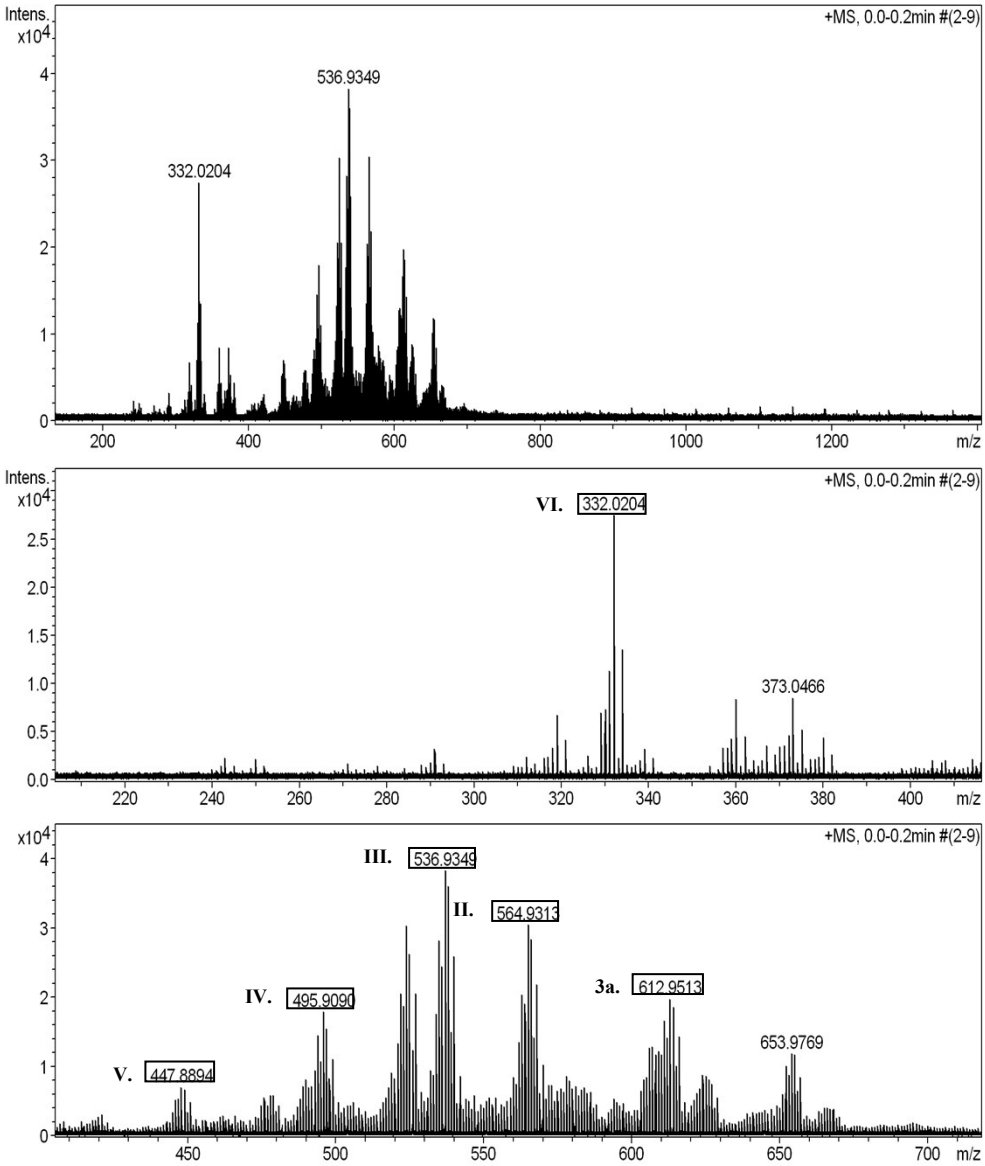

Fig. S10-(9)UV irradiation for 45 minutes

4. Copies of ^{1}H-NMR,^{13}C-NMR and UV-vis spectra

4.1 NMR spectra of Complex 3a-3g

$[Ru_2(CO)_4(\mu^2\text{-}\eta^2\text{-}O_2CCH_3)_2(\eta^1\text{-}NH_2CH_2C(=O)OCH_3)_2]$ (3a)

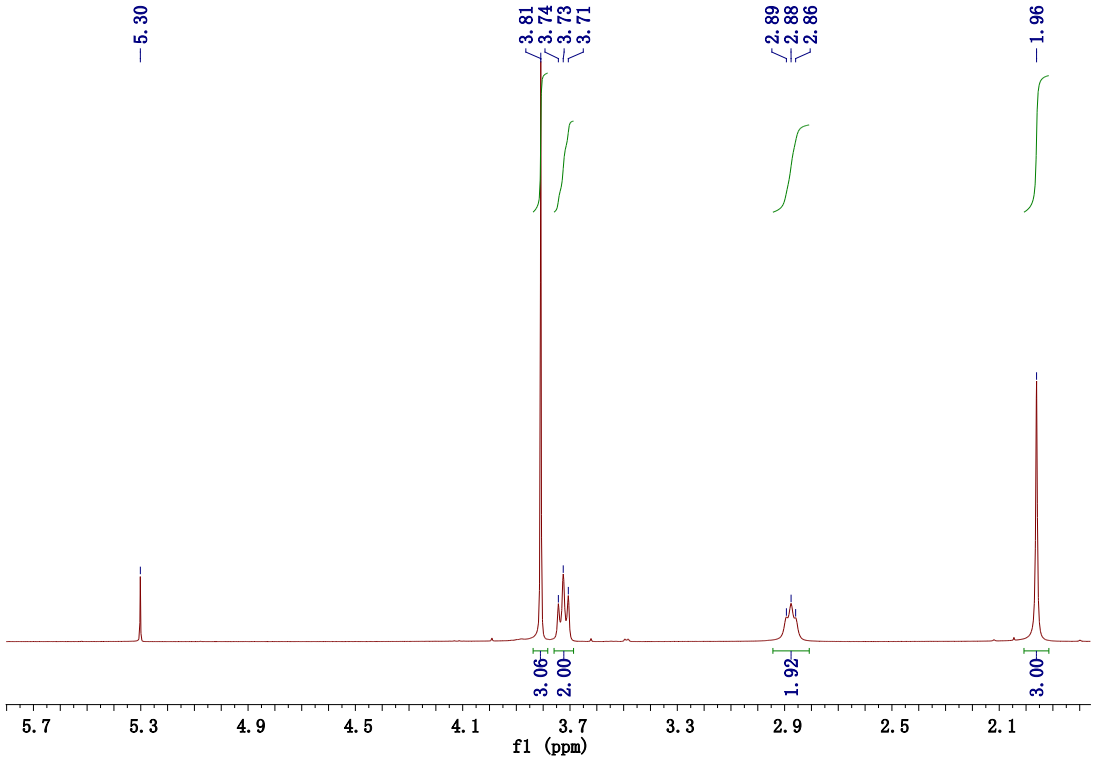

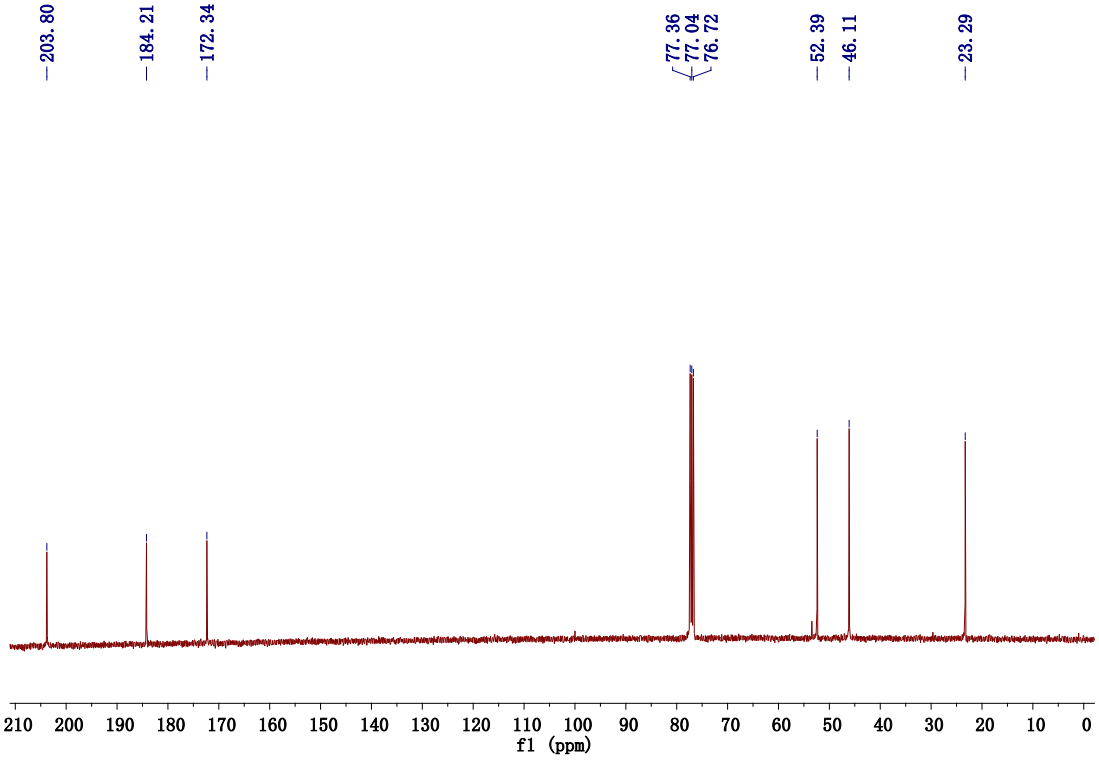

$[Ru_2(CO)_4(\mu^2\text{-}\eta^2\text{-}O_2C\text{-}p\text{-}CH_3C_6H_4)_2(\eta^1\text{-}NH_2CH_2C(=O)OCH_3)_2]$ (3b)

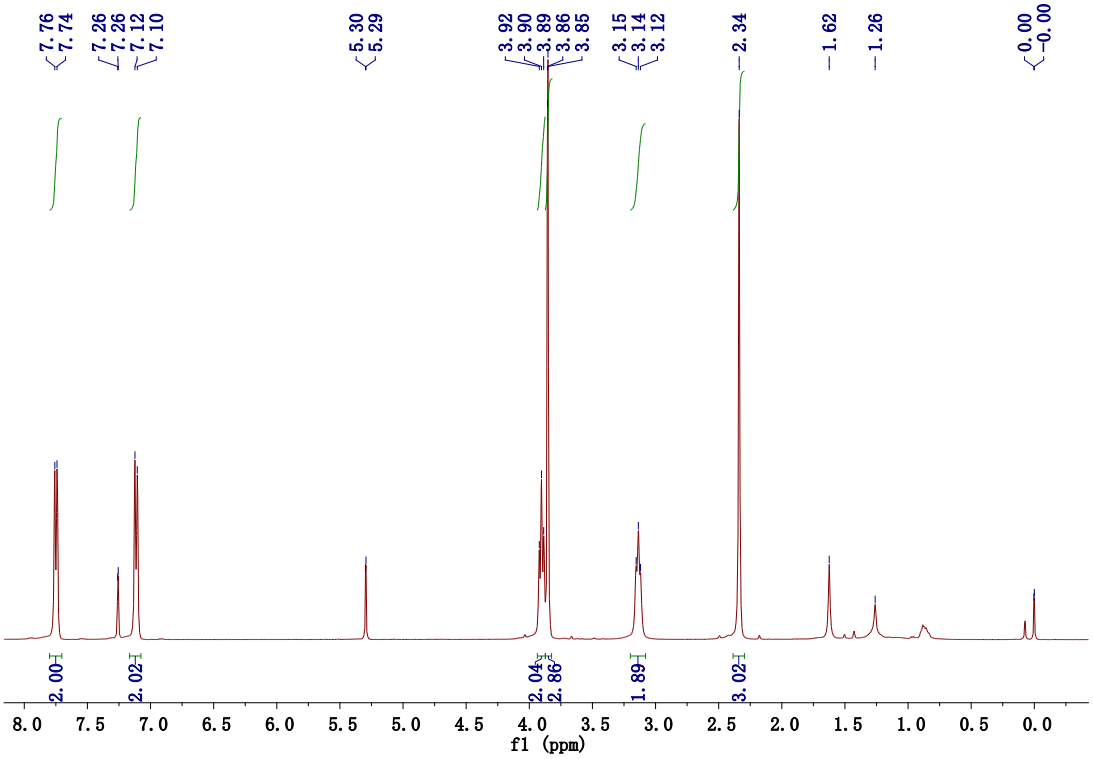

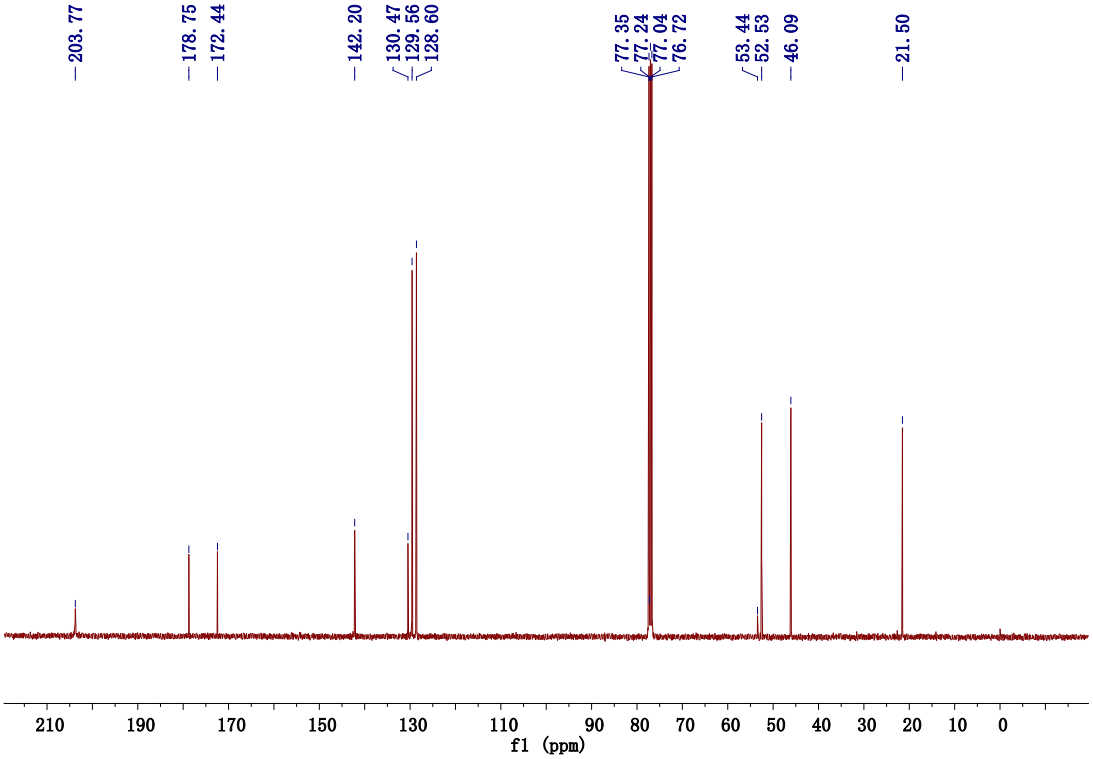

$[Ru_2(CO)_4(\mu^2\text{-}\eta^2\text{-}O_2C\text{-}p\text{-}ClC_6H_4)_2(\eta^1\text{-}NH_2CH_2C(=O)OCH_3)_2)_2]$ (3c)

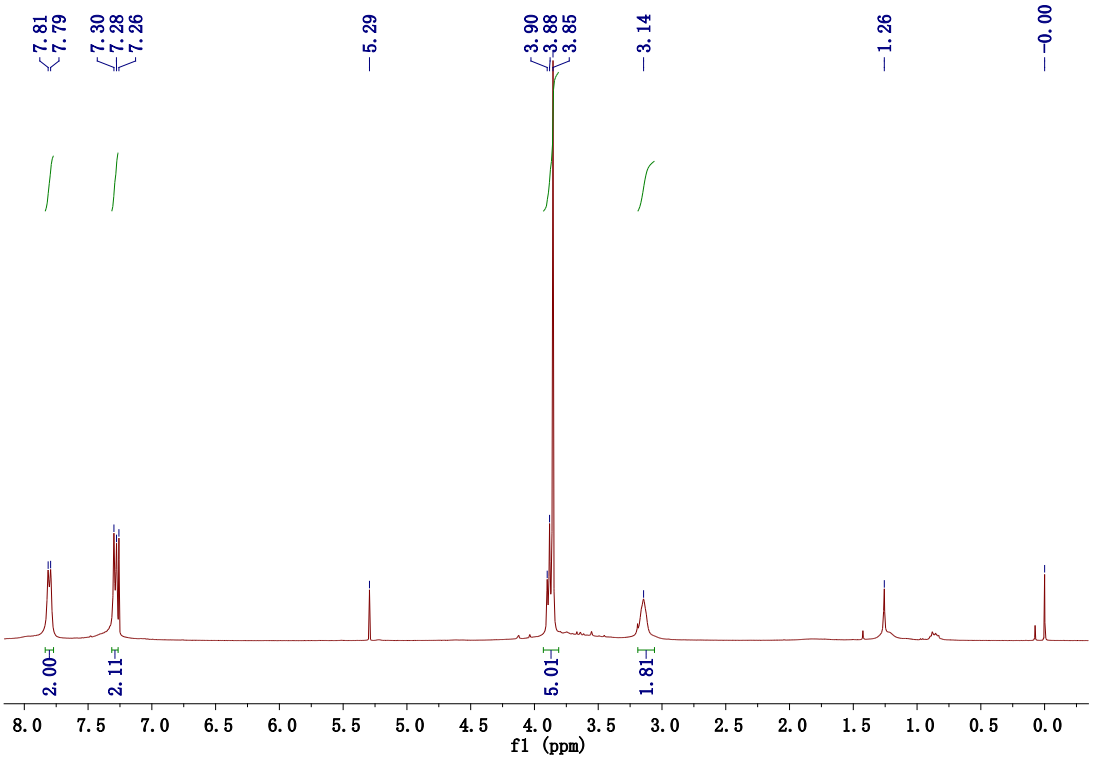

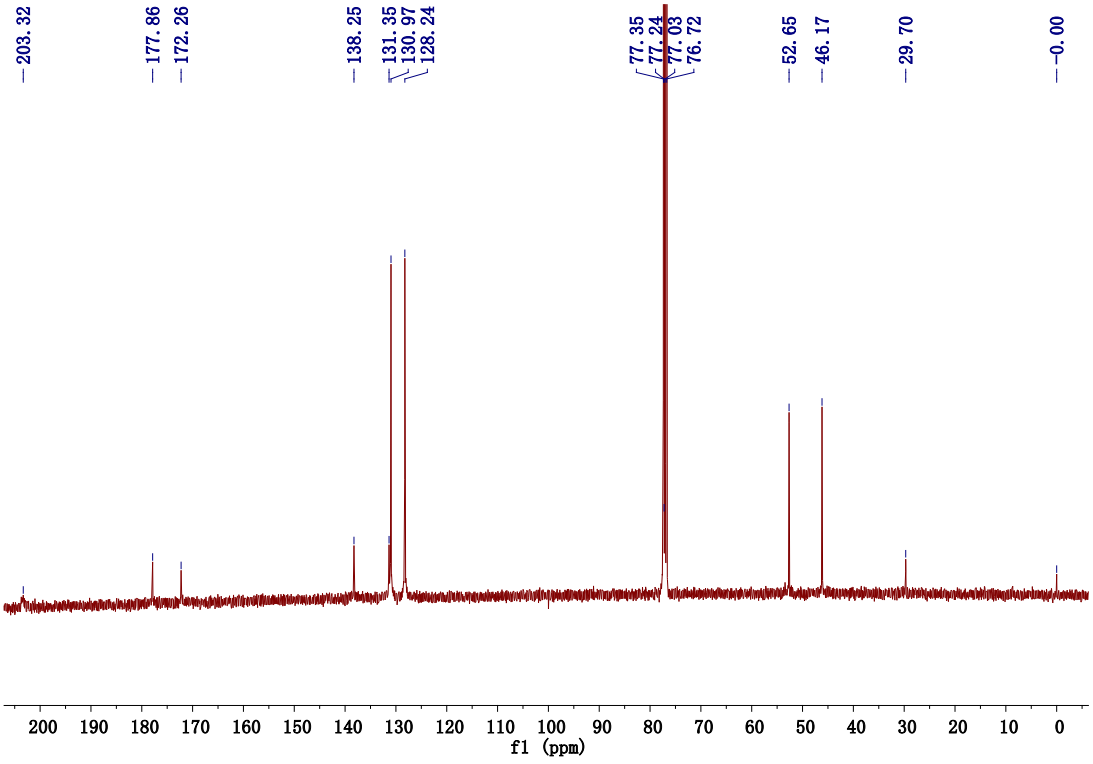

$[Ru_2(CO)_4(\mu^2\text{-}\eta^2\text{-}O_2C\text{-}p\text{-}CH_3OC_6H_4)_2(\eta^1\text{-}NH_2CH_2C(=O)OCH_3)_2]$(3d)

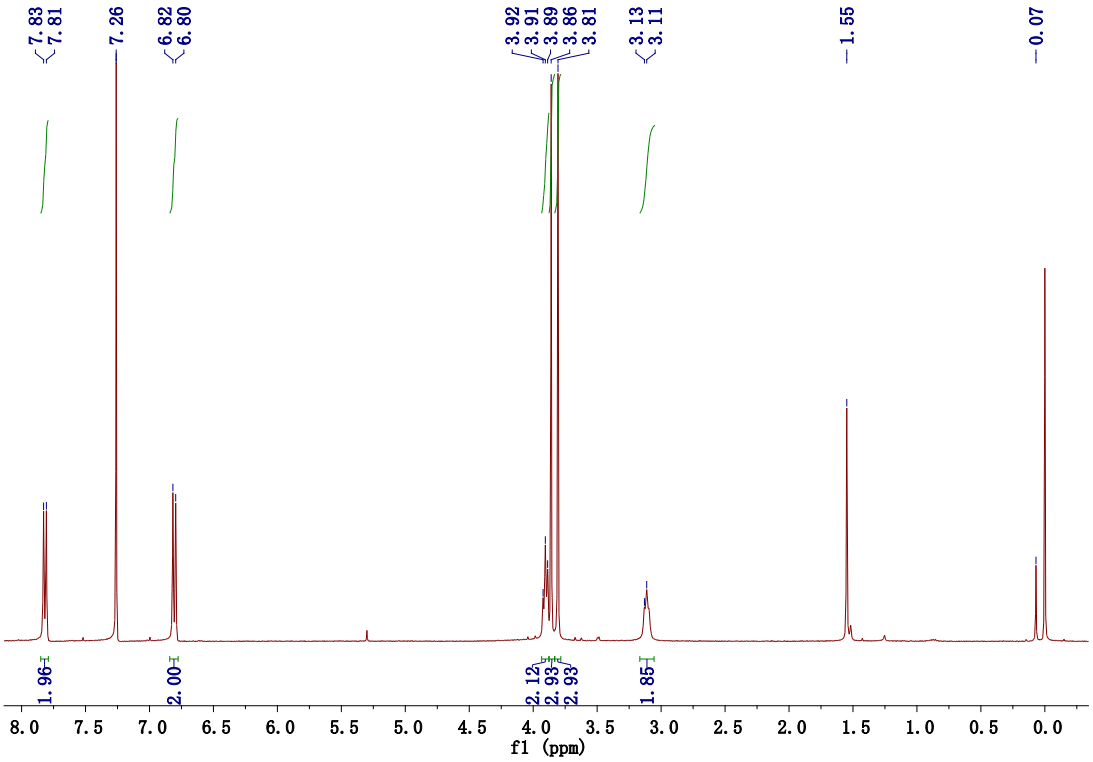

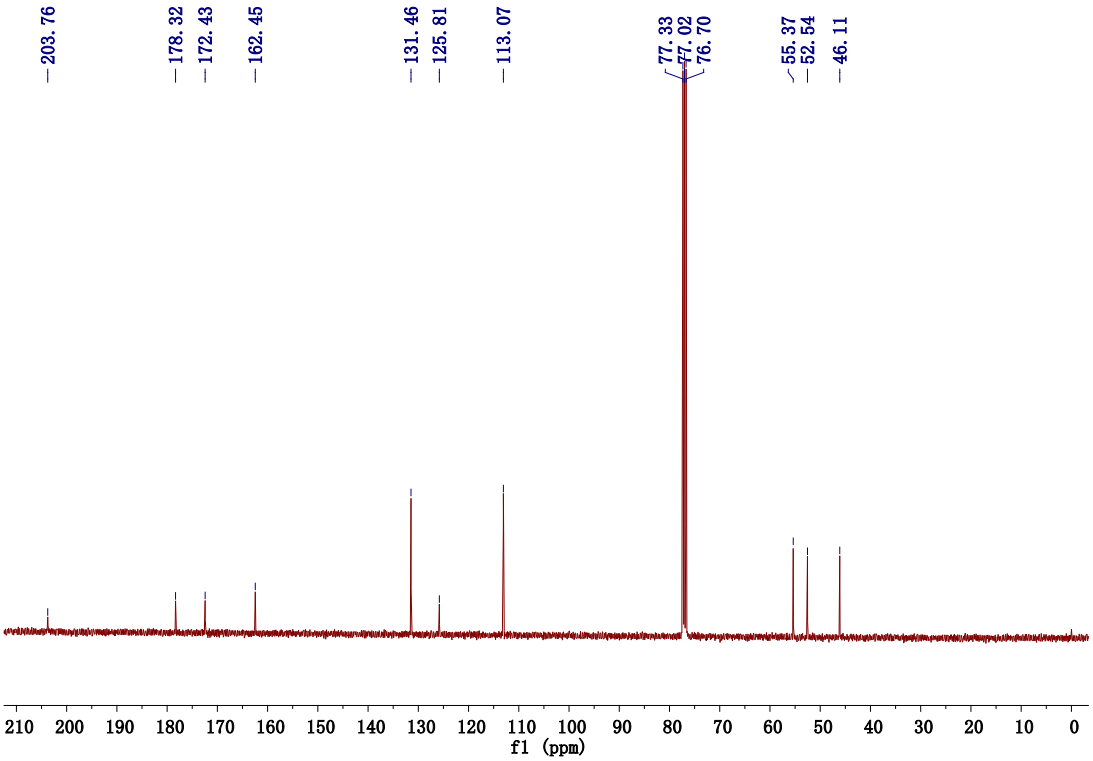

$[Ru_2(CO)_4(\mu^2\text{-}\eta^2\text{-}O_2CC_6H_5)_2(\eta^1\text{-}NH_2CH_2C(=O)OCH_3)_2]$ (3e)

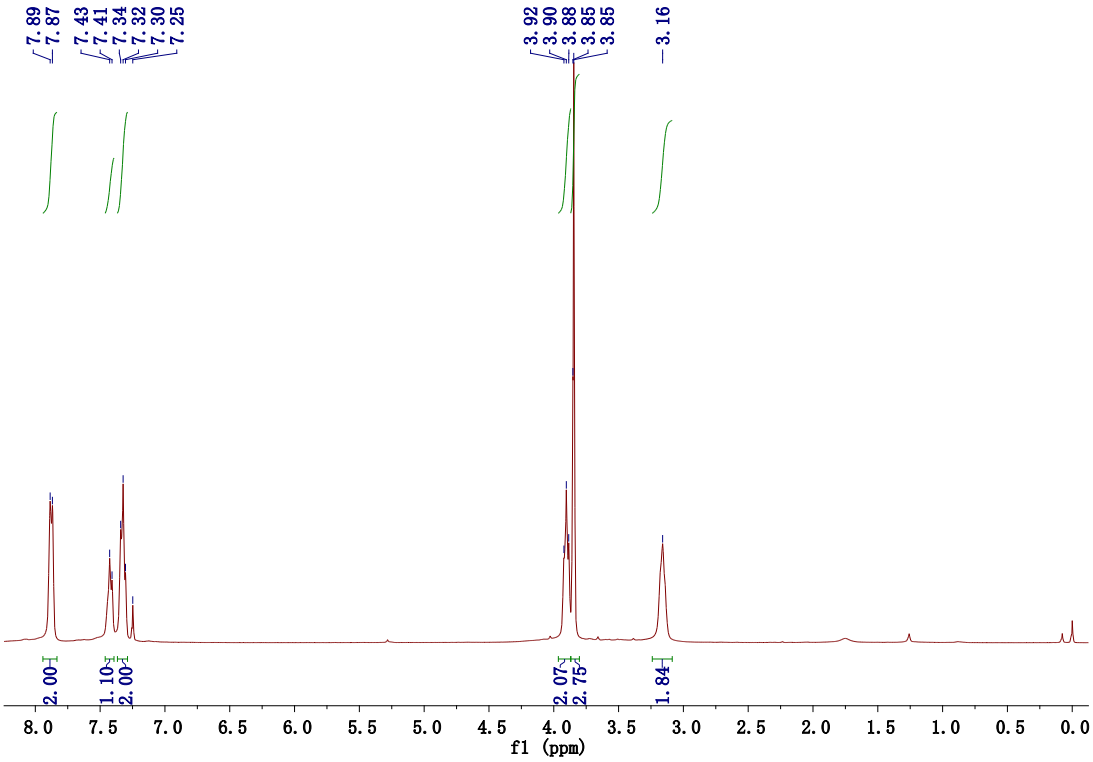

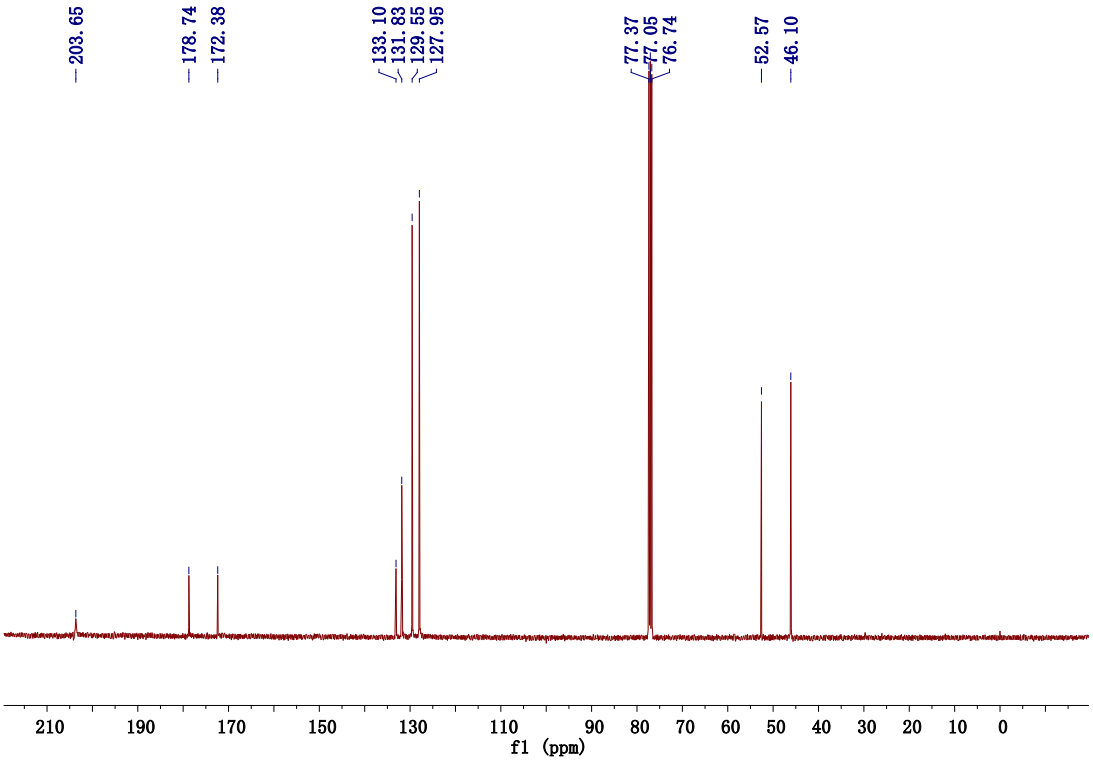

$[Ru_2(CO)_4(\mu^2\text{-}\eta^2\text{-}O_2C\text{-}o\text{-}CH_3C_6H_4)_2(\eta^1\text{-}NH_2CH_2C(=O)OCH_3)_2]$ (3f)

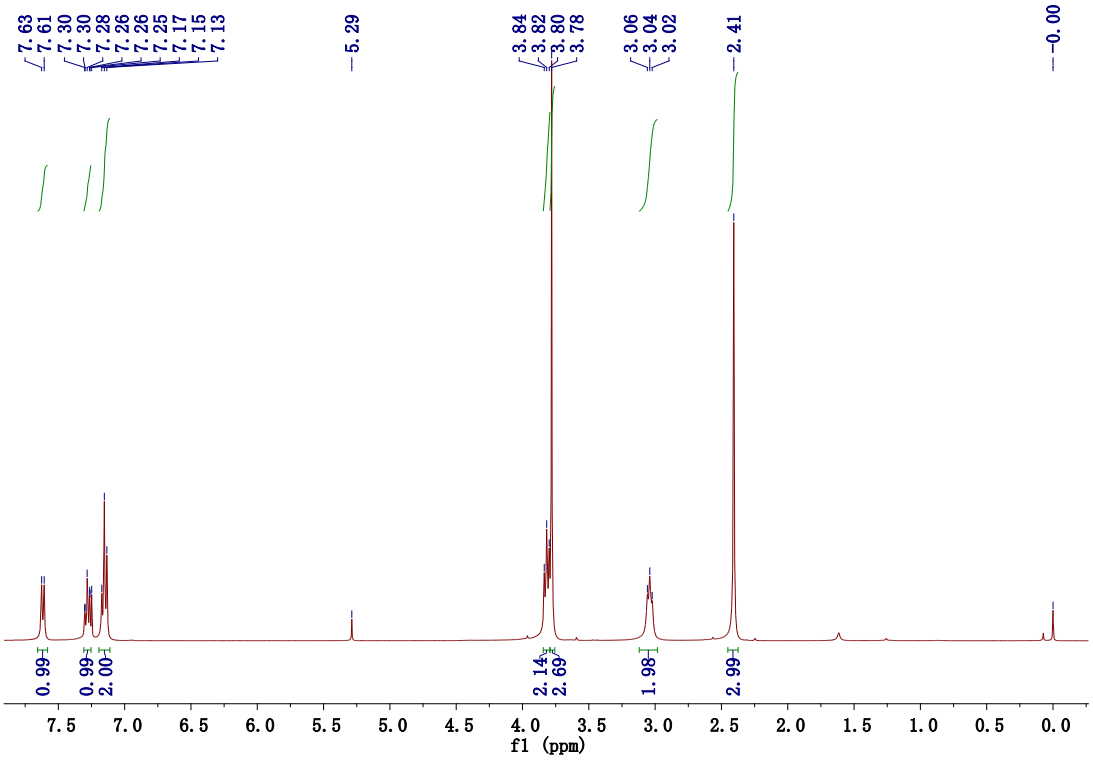

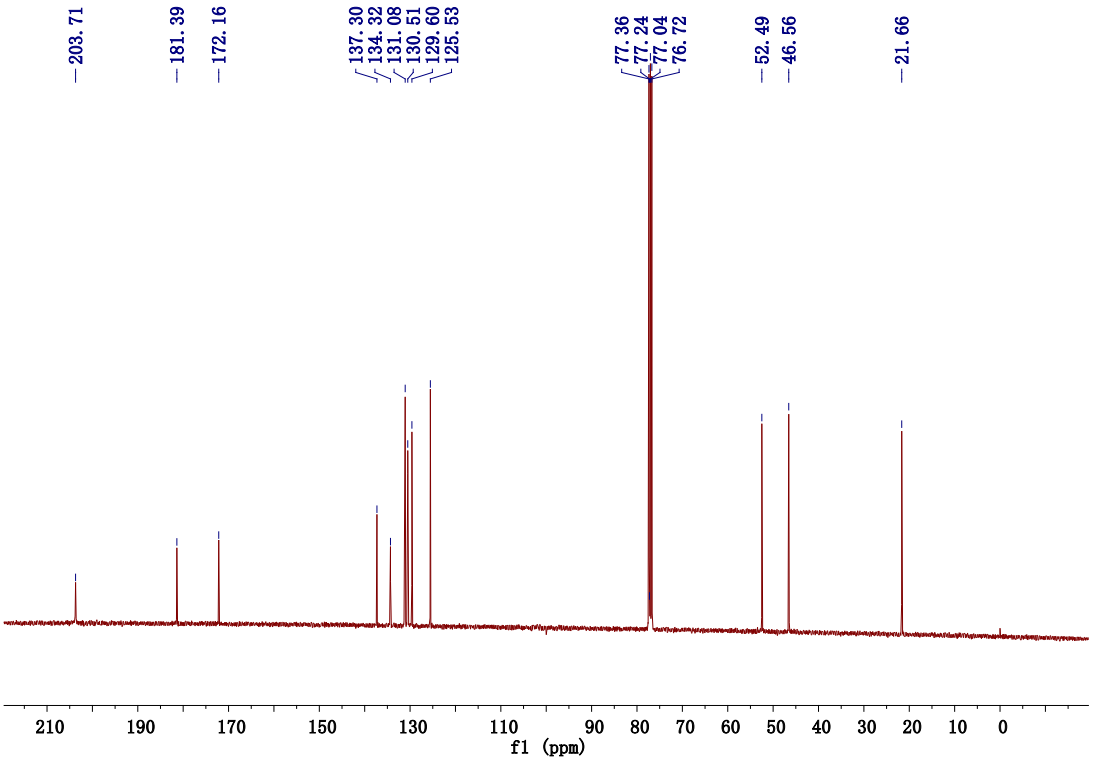

$[Ru_2(CO)_6(\mu^2\text{-}\eta^2\text{-}O_2C\text{-}m\text{-}CH_3C_6H_4)_2(\eta^1\text{-}NH_2CH_2C(=O)OCH_3)_2]$(3g)

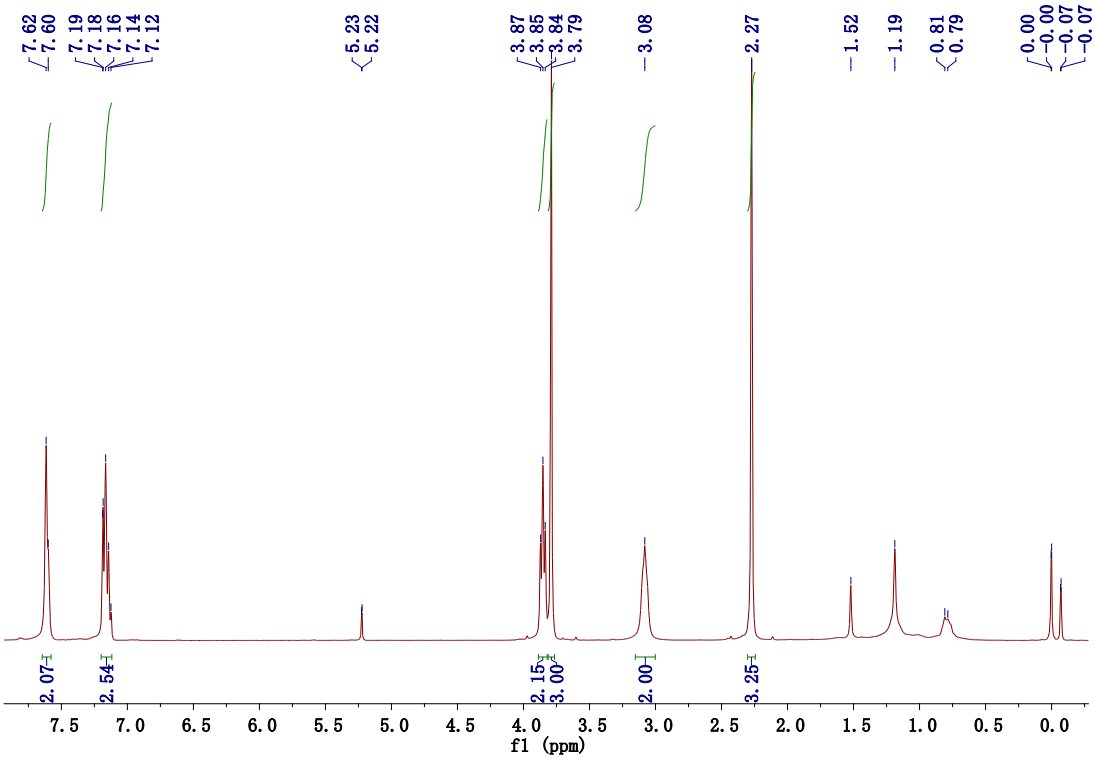

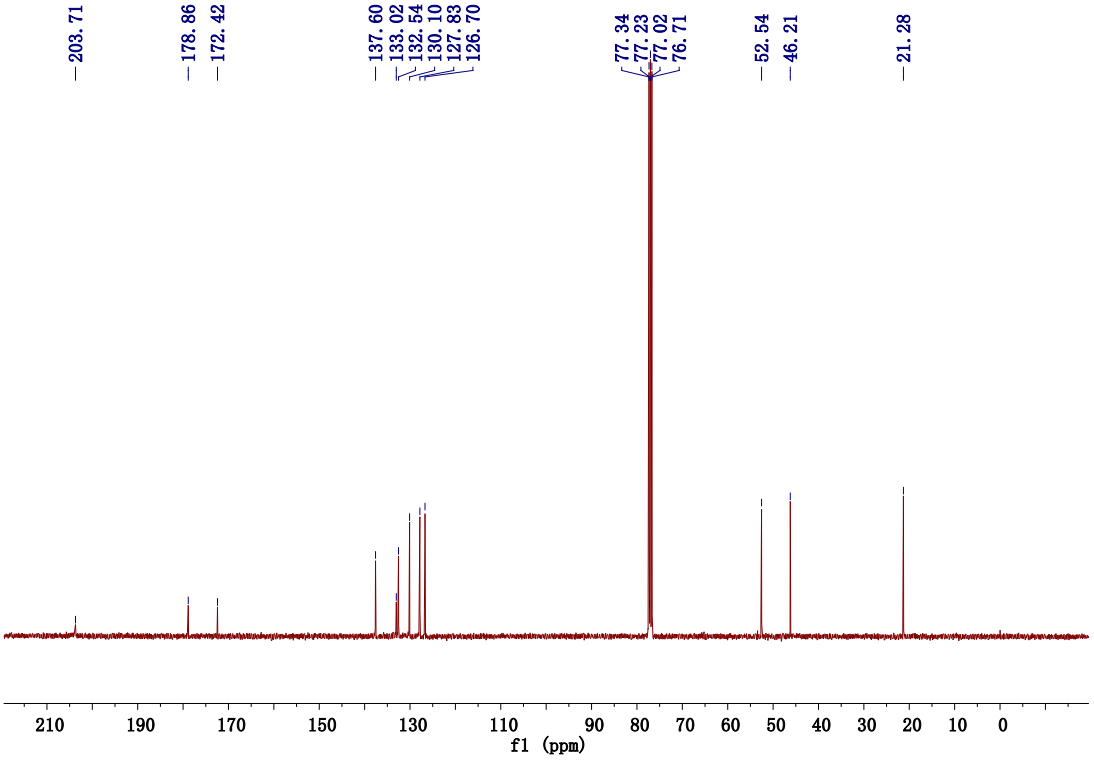

4.2 UV-vis spectra of CO releasing experiments

A typical series of spectra showing the conversion of deoxy-Mb to Mb-CO during light-induced CO dissociation in Fig. S11-(a), (b), (c).The UV-vis spectra therefore allow a quantification of the amount of CO released from the CO-RM with time in Fig. S11-(d).

$[Ru_2(CO)_4(\mu^2\text{-}\eta^2\text{-}O_2CCH_3)_2\ (\eta^1\text{-}NH_2CH_2C(=O)OCH_3)_2]$ (3a)

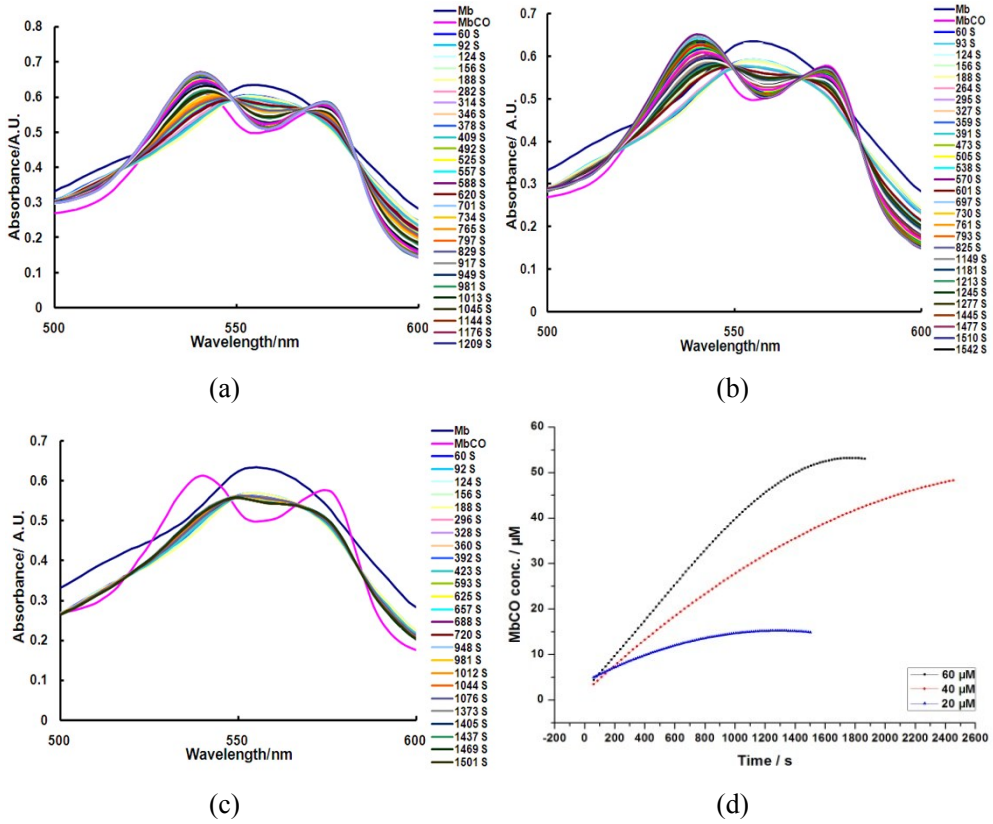

Fig. S11-1 (a), (b), (c) UV-vis spectrum showing the Q-bands during the conversion of deoxy-Mb to Mb-CO with time as CO is released from 3a (60, 40, 20 μM). (d) Plot of [Mb-CO] (60, 40, 20μM) against time.

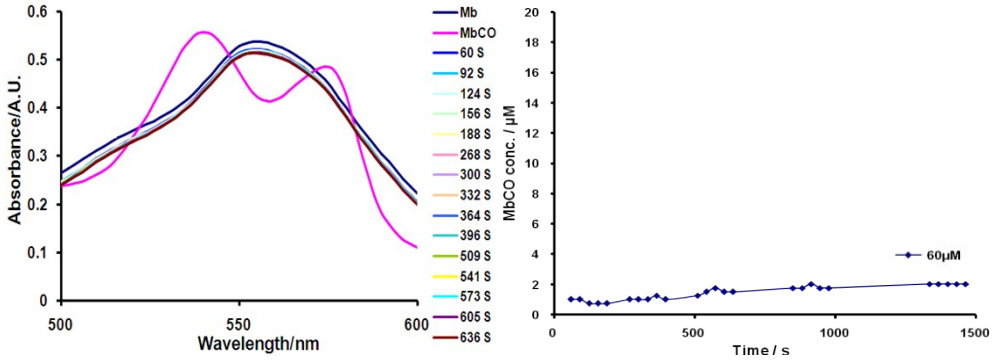

(a) (b)

Fig. S11-2 (a) UV-vis spectrum showing the Q-bands during the conversion ofdeoxy-Mb to Mb-CO in presence of **3a** (60uM) without UV irradiation. (b) Plot of [Mb-CO] against time.

$[Ru_2(CO)_4(\mu^2\text{-}\eta^2\text{-}O_2C\text{-}p\text{-}CH_3C_6H_4)_2(\eta^1\text{-}NH_2CH_2C(=O)OCH_3)_2]$ (3b)

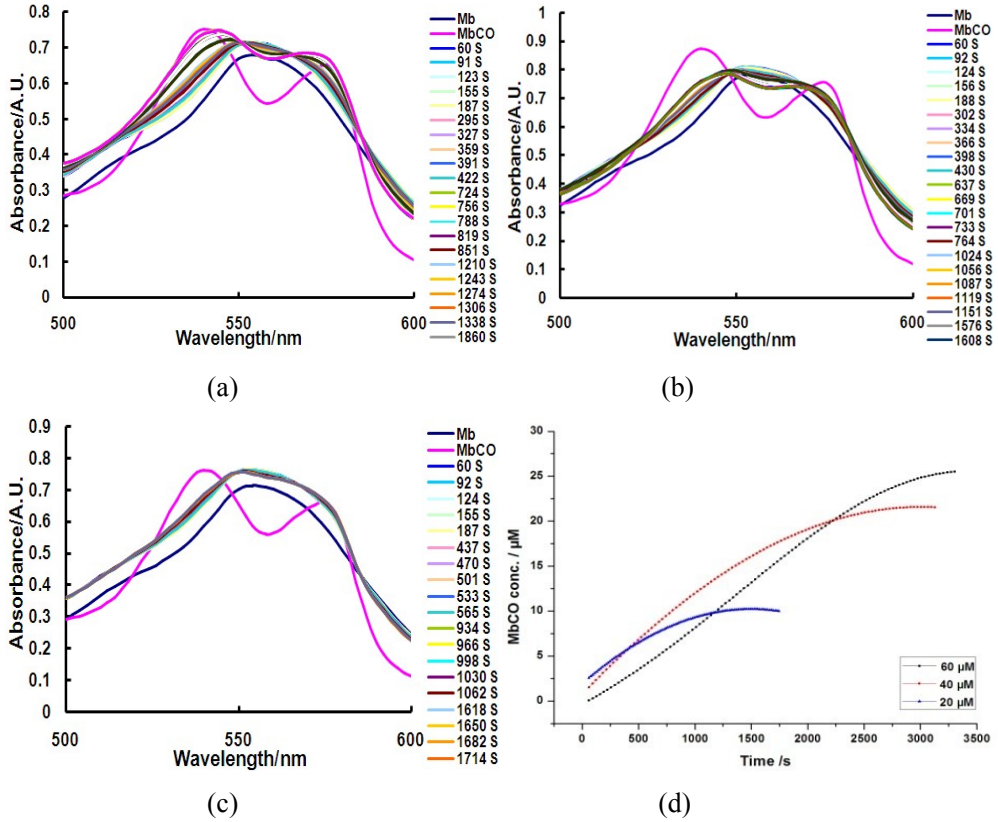

Fig. S11-3 (a), (b), (c) UV-vis spectrum showing the Q-bands during the conversion of deoxy-Mb to Mb-CO with time as CO is released from 3b (60, 40, 20 μM). (d) Plot of [Mb-CO] (60, 40, 20μM) against time.

$[Ru_2(CO)_4(\mu^2\text{-}\eta^2\text{-}O_2C\text{-}p\text{-}ClC_6H_4)_2(\eta^1\text{-}NH_2CH_2C(=O)OCH_3)_2)_2]$ (3c)

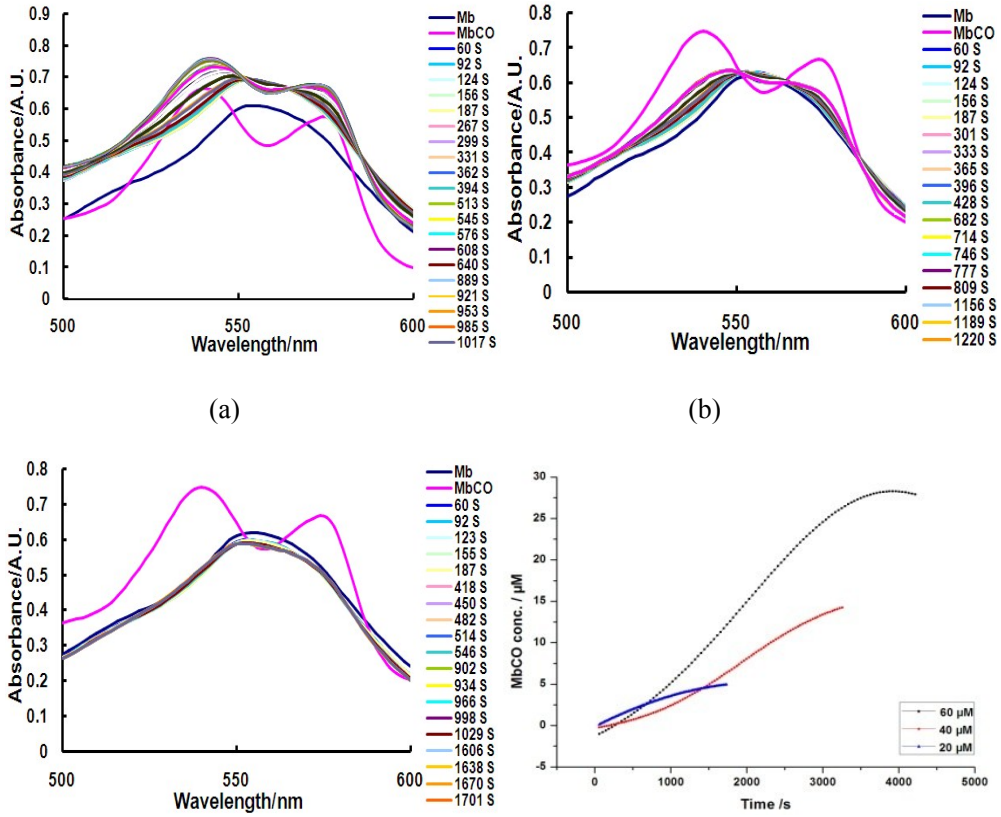

Fig. S11-4 (a), (b), (c) UV-vis spectrum showing the Q-bands during the conversion of deoxy-Mb to Mb-CO with time as CO is released from 3c (60, 40, 20 μM). (d) Plot of [Mb-CO] (60, 40, 20μM) against time.

$[Ru_2(CO)_4(\mu^2\text{-}\eta^2\text{-}O_2C\text{-}p\text{-}CH_3OC_6H_4)_2(\eta^1\text{-}NH_2CH_2C(=O)OCH_3)_2]$ (3d)

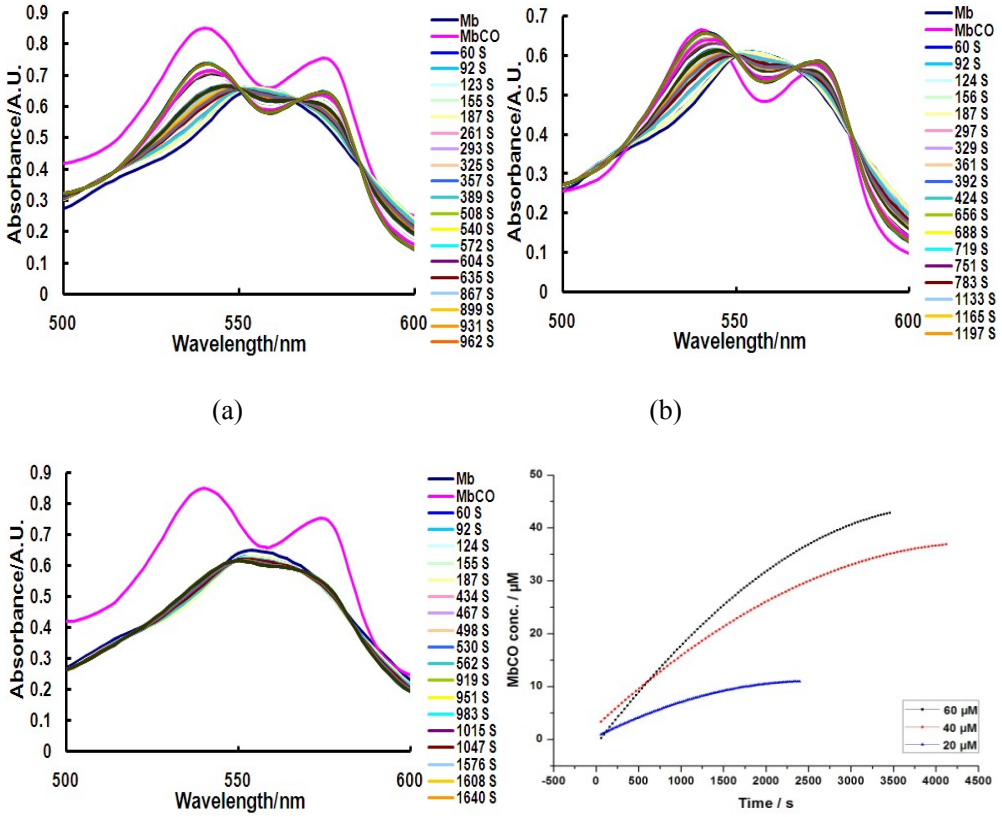

Fig. S11-5 (a), (b), (c) UV-vis spectrum showing the Q-bands during the conversion of deoxy-Mb to Mb-CO with time as CO is released from 3d (60, 40, 20 μM). (d) Plot of [Mb-CO] (60, 40, 20μM) against time.

$[Ru_2(CO)_4(\mu^2\text{-}\eta^2\text{-}O_2CC_6H_5)_2(\eta^1\text{-}NH_2CH_2C(=O)OCH_3)_2]$ (3e)

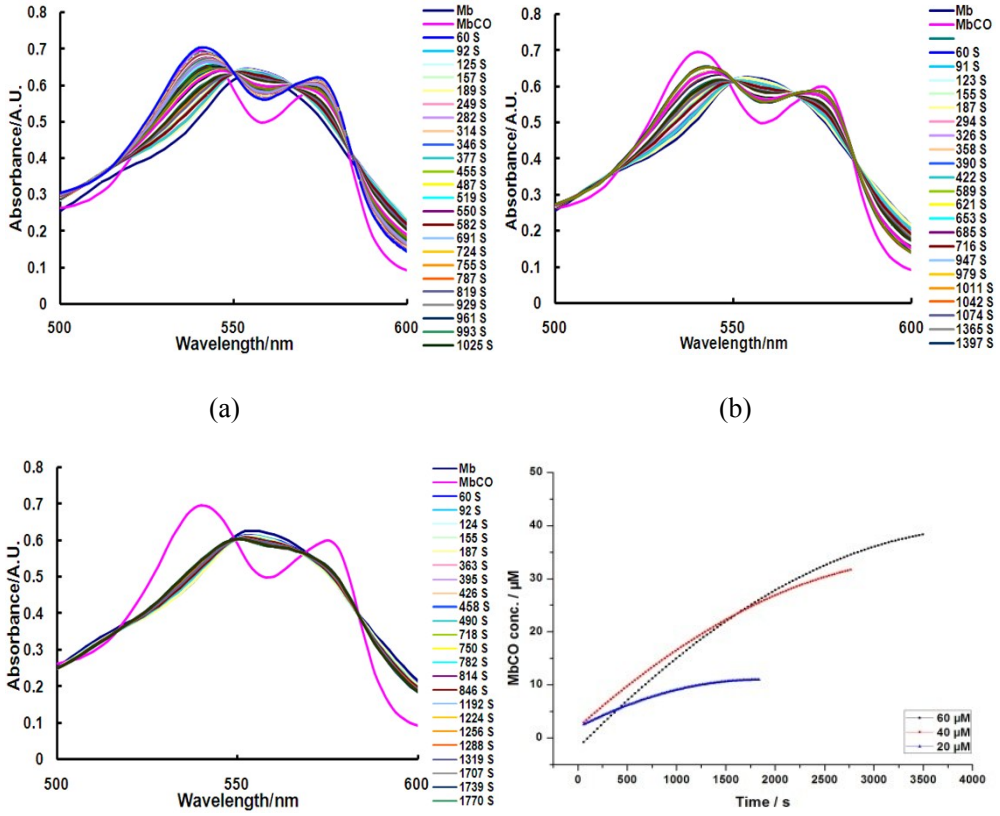

Fig. S11-6 (a), (b), (c) UV-vis spectrum showing the Q-bands during the conversion of deoxy-Mb to Mb-CO with time as CO is released from 3e (60, 40, 20 μM). (d) Plot of [Mb-CO] (60, 40, 20μM) against time .

$[Ru_2(CO)_4(\mu^2\text{-}\eta^2\text{-}O_2C\text{-}o\text{-}CH_3C_6H_4)_2(\eta^1\text{-}NH_2CH_2C(=O)OCH_3)_2]$ (3f)

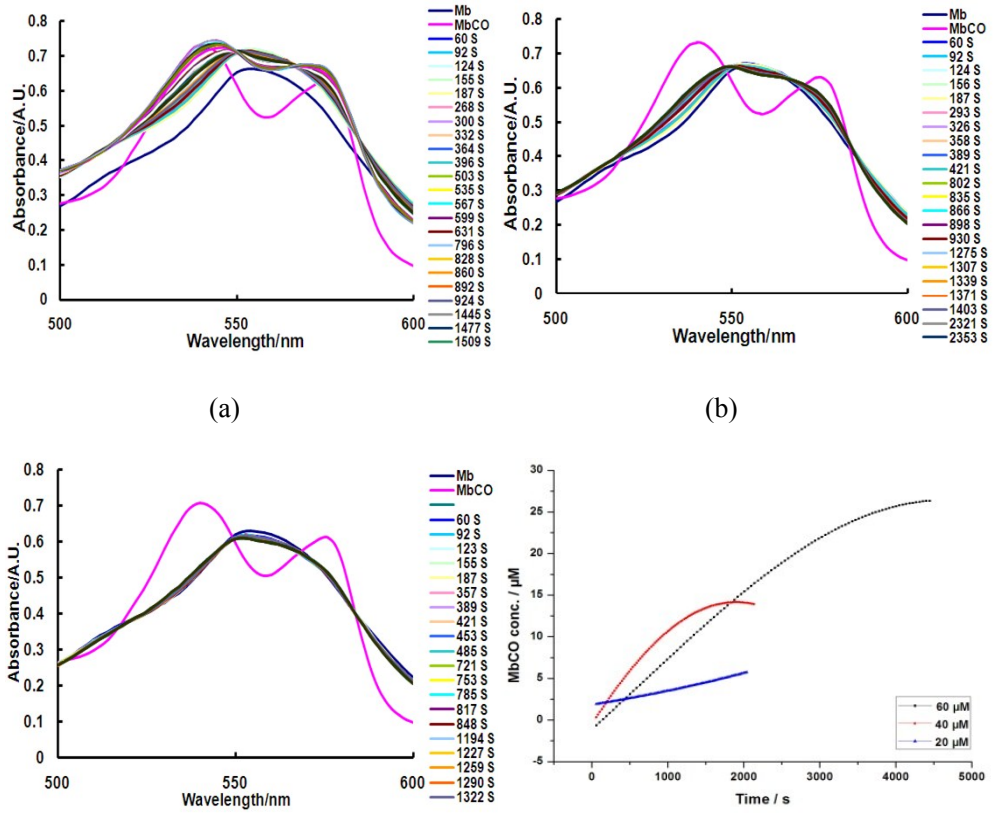

Fig. S11-7 (a), (b), (c) UV-vis spectrum showing the Q-bands during the conversion of deoxy-Mb to Mb-CO with time as CO is released from 3f (60, 40, 20 μM). (d) Plot of [Mb-CO] (60, 40, 20μM) against time.

$[Ru_2(CO)_4(\mu^2\text{-}\eta^2\text{-}O_2C\text{-}m\text{-}CH_3C_6H_4)_2(\eta^1\text{-}NH_2CH_2C(=O)OCH_3)_2]$ (3g)

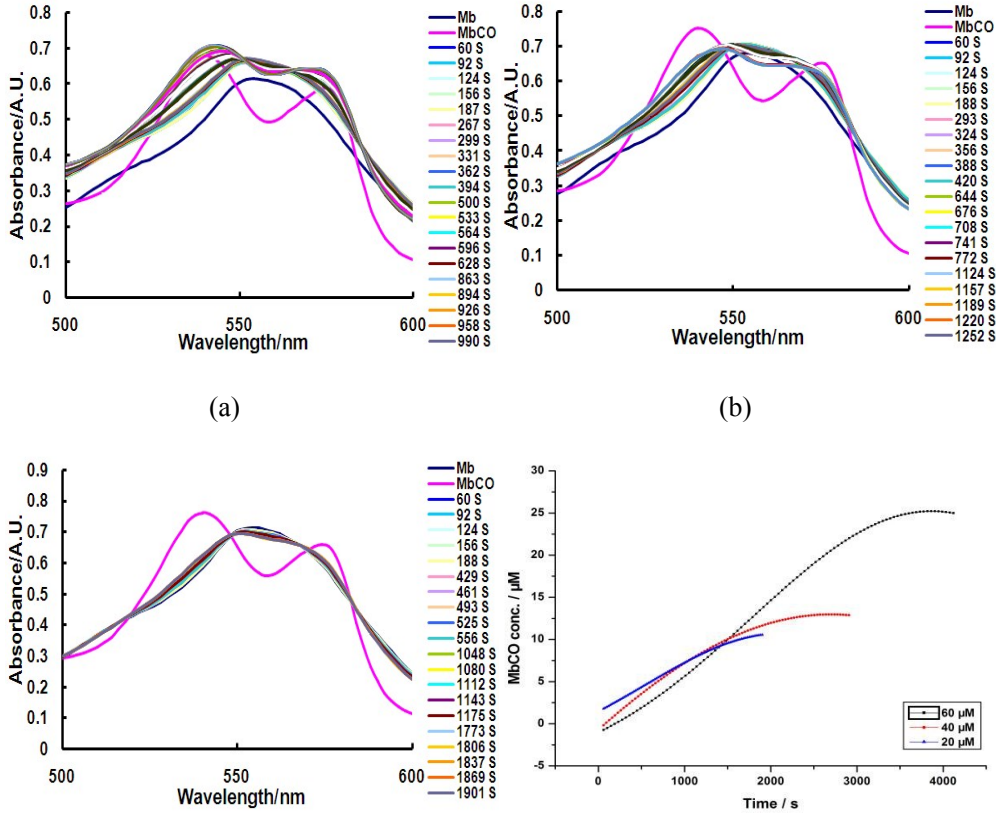

Fig. S11-8 (a), (b), (c) UV-vis spectrum showing the Q-bands during the conversion of deoxy-Mb to Mb-CO with time as CO is released from 3g (60, 40, 20 µM). (d) Plot of [Mb-CO] (60, 40, 20µM) against time.

4.3 UV-vis spectra of 3a-3g

UV-vis spectra of **3a-3g** in CH_3CN were showed in Fig. S12.

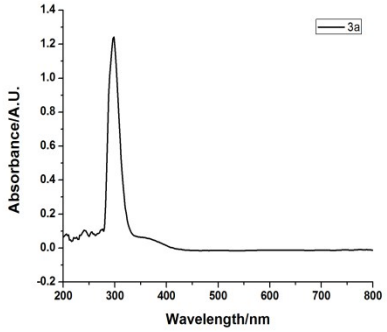

Fig. S12(a) UV-vis spectra of **3a**.

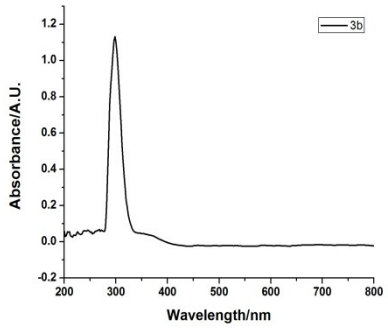

Fig. S12(b) UV-vis spectra of **3b**.

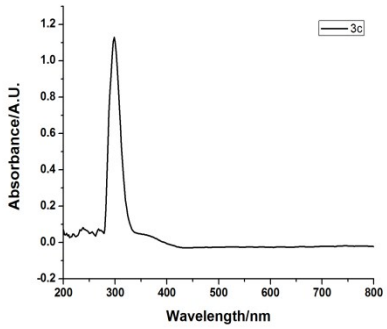

Fig. S12(c) UV-vis spectra of **3c**.

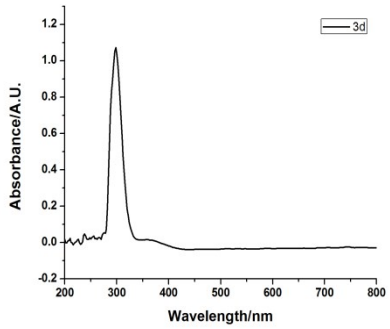

Fig. S12(d) UV-vis spectra of **3d**.

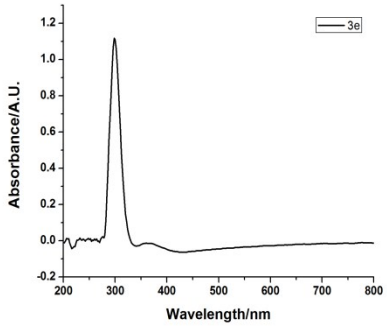

Fig. S12(e) UV-vis spectra of **3e**.

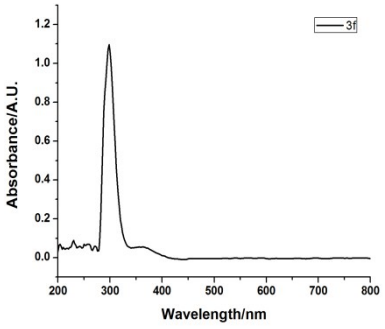

Fig. S12(f) UV-vis spectra of **3f**.

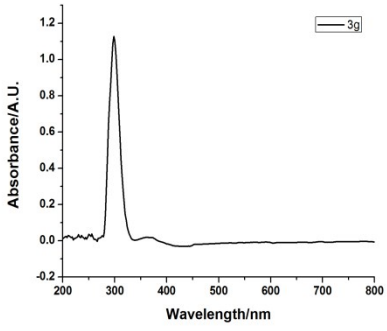

Fig. S12(g) UV-vis spectra of **3g**.

5. Cell culture and Cytotoxicity studies

Murine RAW264.7 macrophages cells were used for preliminary cytotoxicity studies. Take the cryopreserved RAW264.7 cell line at 37 ºC quickly thawed, then centrifugal 5 min at 1000 r/min and clean 1~2 times by FBS medium because in the process of frozen joined the harmful substances for the growth of cell reproduction. Centrifugation after resuspension with FBS medium. Add the culture medium in RAW264.7 cells which changed every day. After cells growth long full which can used backup.

Storage solutions of CORMs **3a** and **3f** were prepared in DMSO (10 mol/L) and diluted with DMEM culture medium in the concentration range from 10 μM to 1000 μM. RAW264.7 cells were seeded in 96-well plates at 5×10^3 cells per well and the cells were incubated in 5% CO_2 for 24 h at 37 ºC. Then, **3a** or **3f** at different concentrations (150μL) were incubated with RAW264.7 cells for 2h in three 96-well plates, respectively. The cells which irradiated for 15min with 365 nm light or not placed in the dark for 8h measured by MTT assay.

Every 96-well plate was added 15 μL MTT, then the cells were incubated in 5% CO_2 for 3~4 h at 37 ºC. Remove the plates liquid, adding 200μL DMSO and shaking 10 min at room temperature. The OD value of same time was measured using a Enzyme mark detector (Thermo MK3) with an excitation wavelength of 420 nm.

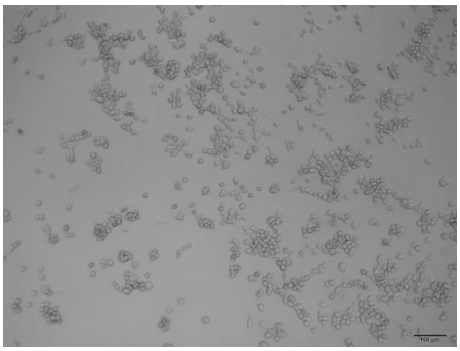

Fig. S13 Photo of cells were incubated in the control.

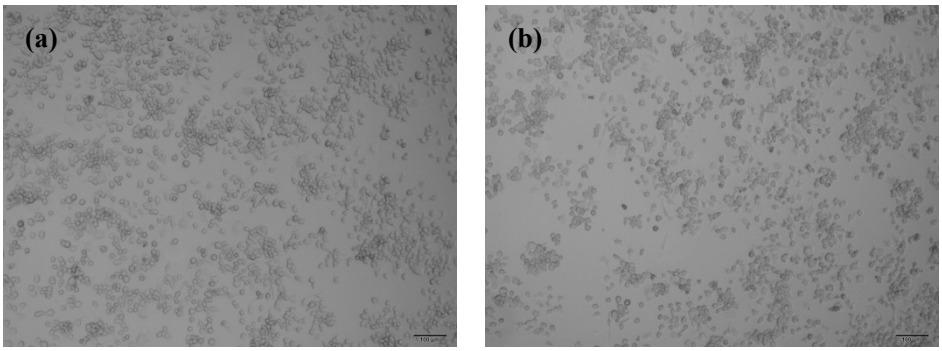

Fig. S14 Photo of cells were incubated at the concentration of 500μM of **3a**. (a) Cells in the dark. (b) Cells irradiated at 365 nm for 15 min.

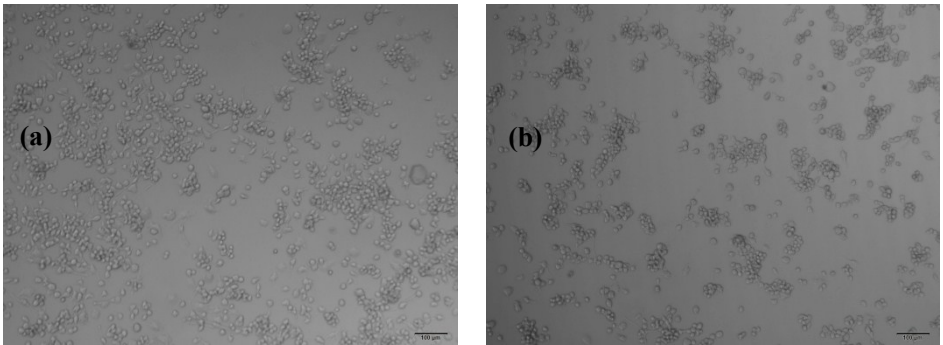

Fig. S15 Photo of cells were incubated at the concentration of 10μM of **3f**. (a) Cells in the dark. (b) Cells irradiated at 365 nm for 15 min.

References for Supplementary Information

1. G. M. Sheldrick, SADSAB, Program for Area Detector Adsorption Correction, Instute for Innorganic Chemistry. University of Gottingen, Germany. 1996.
2. G. M. Sheldrick, SHELEXL-97, Program for Solution of Crystal Structures. University of Gottingen, Germany. 1997.
3. W. Q Zhang, A. J. Atkin, R. J. Thatcher, A. C. Whitwood, I. J. S. Fairlamb, J. M. Lynam, *Dalton Trans.*, 2009, 4351 – 4358.